Quaternary Science Reviews 266 (2021) 107078

Contents lists available at ScienceDirect

Quaternary Science Reviews

journal homepage: www.elsevier.com/locate/quascirev

An extension of the TALDICE ice core age scale reaching back to MIS 10.1

Ilaria Crotti [a, b, *], Amaelle Landais [b], Barbara Stenni [a, f], Lucie Bazin [b], Frédéric Parrenin [c], Massimo Frezzotti [d], Florian Ritterbusch [e], Zheng-Tian Lu [e], Wei Jiang [e], Guo-Min Yang [e], Elise Fourré [b], Anais Orsi [b], Roxanne Jacob [b], Bénédicte Minster [b], Frédéric Prié [b], Giuliano Dreossi [f], Carlo Barbante [a, f]

[a] Department of Environmental Sciences, Informatics and Statistics, Ca' Foscari University, Venice, 30172, Italy
[b] Laboratoire des Sciences du Climat et de l'Environnement LSCE/IPSL, CEA-CNRS-UVSQ, Université Paris-Saclay, 91191, Gif-sur-Yvette, France
[c] University Grenoble Alpes, CNRS, IRD, IGE, 38058, Grenoble, France
[d] Department of Science, Roma Tre University, Rome, 00154, Italy
[e] University of Science and Technology of China, Hefei, 230026, China
[f] Institute of Polar Sciences (ISP), CNR, Venice, 30172, Italy

ARTICLE INFO

Article history:
Received 30 March 2021
Received in revised form
22 June 2021
Accepted 1 July 2021
Available online xxx

Handling Editor: C. O'Cofaigh

Keywords:
Ice core chronology
East Antarctica
^{81}Kr dating

ABSTRACT

TALDICE (TALos Dome Ice CorE) is a 1620 m deep ice core drilled at Talos Dome, an ice dome located at the edge of the East Antarctic Plateau in the Ross Sea Sector. The Antarctic Ice Core Common Chronology (AICC2012) extended the age scale of the core until ~150 ka (1438 m depth) (Bazin et al., 2013), while no age scale was available below 1438 m depth.

In this work we present the new TALDICE-deep1 chronology using the new measurements of $\delta^{18}O_{atm}$, δD and ^{81}Kr as well as the inverse model IceChrono1.

The TALDICE-deep1 chronology stops at 1548 m, as the portion below this depth is probably affected by mixing processes. The new age scale extends the climate record for the Ross Sea Sector of the East Antarctic Ice Sheet back to MIS 10.1−343 ka (1548 m depth) and identifies both MIS 7 and 9 warm stages, which show specificities in the δD signal. However, it is not possible to recover the isotopic record beyond stage 10.1 as the signal shows a *quasi-flat* shape. Thereby, the new chronology TADICE-deep1 doubles the extension of the previous age scale as it covers the three past glacial/interglacial cycles.

1. Introduction

Because of ice thinning from the top to the bottom of the ice-sheet, the deepest sections of ice cores store most of the paleoclimatic information. However, phenomena acting in the lowermost layers of ice-sheets, such as strong diffusion and physical layer mixing, may affect the quality of the record and its interpretation (NEEM community members, 2013; Tison et al., 2015). Improving dating techniques for the deeper sections of ice cores, as well as extending climate records further back in time, represents one of the major challenges of the ice core science community, which is now involved in the quest of the oldest ice core (Lilien et al., 2021; Parrenin et al., 2017).

The low accumulation rates of ice core drilling sites on the East Antarctic plateau prevent annual layer counting. Consequently, deep ice cores need the employment of dating strategies based on various approaches combining age markers of gas and ice phases (e.g. volcanic tephra) with ice flow modelling (Parrenin et al., 2007; Bazin et al., 2013). Some tracers provide absolute or orbital dating constraints, i.e., dating constraints for each individual ice core, while other tracers provide relative dating constraints, i.e., stratigraphic tie points, to adjust the timescale of one ice core relative to another ice core age scale.

Air trapped in polar ice cores has the unique property of containing global tracers of the atmosphere, which record the variations of atmospheric composition over time at different drilling sites in both hemispheres (Loulergue et al., 2008; Petit et al., 1999; Raynaud et al., 1993). The $\delta^{18}O$ of atmospheric O_2 ($\delta^{18}O_{atm}$) and CH_4

* Corresponding author. Department of Environmental Sciences, Informatics and Statistics, Ca' Foscari University, Venice, 30172, Italy.
E-mail addresses: ila.crotti@unive.it, ilaria.crotti@lsce.ipsl.fr (I. Crotti).

https://doi.org/10.1016/j.quascirev.2021.107078
0277-3791/

represent two signals well suited to define relative age scales for different ice cores through records synchronization. $\delta^{18}O_{atm}$ is characterized by an atmospheric turnover time on the order of 1000–2000 years and can be used to provide tie points on millennial and multi-millennial timescales (Capron et al., 2010), while CH_4 is characterized by a much shorter residence time (5–10 years) and is used for synchronization on multidecadal to millenial timescales if sampling resolution and width of the age distribution allows for.

In addition to gas synchronization tools, some independent absolute constraints can be obtained. Radiometric dating, based on the well-known radioactive decay of certain isotopes, represents an alternative and complementary dating technique. Recent instrumental developments have enabled the use of ^{81}Kr (229,000 years half-life) for dating ice cores. Its dating range of 0.03–1.3 Ma (million years) perfectly fits the expected age range of Antarctic ice. As a noble gas isotope, it is not involved in complicated geochemical reactions and it is well mixed in the atmosphere (Lu et al., 2014). Moreover, the anthropogenic ^{85}Kr can be measured simultaneously with ^{81}Kr to quantify any contamination with modern air.

However, absolute dating and gas records cannot not be employed alone to construct ice core age scales and they are frequently associated with glaciological modelling to build robust chronologies. The most common modelling approach for Antarctic ice cores is based on the application of Bayesian tools such as, the Datice or IceChrono1, respectively developed by Lemieux-Dudon et al. (2010) and Parrenin et al. (2015), which compute the best compromise between markers (absolute and relative) and prior estimation of the ice and gas chronologies (background scenario). The background scenario consists in the estimation of depth-profiles of three glaciological quantities: accumulation rate, thinning function and Lock-In-Depth (LID). The LID corresponds to the lowermost depth where air can diffuse in the firn (Buizert et al., 2013; Landais et al., 2006). The calculation of the LID is essential for dating purpose, as it provides a tool to link gas and ice chronologies. A first determination of this depth can be estimated from a firn densification model adapted to the surface characteristics of the site of interest (Bréant et al., 2017). Measurements of $\delta^{15}N$ of molecular N_2 also provide constraints on the LID: because of the effect of gravity, $\delta^{15}N$ in the firn air, and thus enclosed in air bubbles, is proportional to the LID at the time of depth enclosure in absence of any abrupt mean temperature change (Severinghaus et al., 1998). An ice flow model (e.g. Parrenin et al., 2004) provides an estimation of the thinning function using scenario of past temperature and accumulation rate as well as temperature profile in depth. δD or $\delta^{18}O$ profiles are used to calculate the accumulation rate (Parrenin et al., 2007).

TALDICE (TALos Dome Ice CorE) is a 1620 m deep ice core drilled at Talos Dome, an ice dome located on the edge of the East Antarctic plateau, about 290 km from the Southern Ocean, 250 km from the Ross Sea, 275 km from the Italian Mario Zucchelli Station, 550 km North of Taylor Dome, 1500 km NW of Siple Dome, and 1100 km East of Dome C (Frezzotti et al., 2004). The drilled core is longer than expected since the target area was missed by less than 200 m and the bedrock was not reached. The drilling reaches a 1.6 km wide valley, not noticed in the low-resolution radar profiles available at that time and spotted later in high resolution radar surveys (Figure 1b). The ice thickness at the drilling site is ~1795 m, surrounded by subglacial hills at about 1550 m (Jordan et al., 2008).

The first official age scale for the TALDICE core, TALDICE-1, is defined by Buiron et al. (2011), combining glaciological modelling to CH_4 and $\delta^{18}O_{atm}$ records synchronization with already dated ice cores from Antarctica and Greenland. The dating method is based on the Datice tool (Lemieux-Dudon et al., 2010). The TALDICE-1 chronology is built only until 1428 m depth, corresponding to a gas age of ~141 ka (thousands of years before present) due to the low resolution of the available $\delta^{18}O_{ice}$ and CH_4 records (Buiron et al., 2011). In order to reduce the uncertainties associated with the first age scale, Schüpbach et al. (2011) propose TALDICE 1-a, a refined age scale covering the time span between 55 and 112 ka (1293–1380 m depth), based on new high-resolution methane data produced by Continuous Flow Analysis (CFA). The new CH_4 measurements allow the reduction of the uncertainties associated with the age scale from 1.9 ka in TALDICE-1 to 1.1 ka in the considered time interval. Then, the TALDICE chronology is improved a third time and included in the AICC2012 (Antarctic Ice Core Chronology, 2012) framework (Bazin et al., 2013; Veres et al., 2013), a multi-proxy and multi-site ice and gas orbital chronology which spans the last 800 ka. AICC2012 is based on the same dating strategy applied for TALDICE-1 (Datice model and synchronization), including several new gas measurements for all involved cores. For TALDICE, new $\delta^{18}O_{atm}$ measurements extend the record of Buiron et al. (2011) from 1402 m down to 1553.95 m depth. Despite the novel gas record, the poor resolution of both methane and $\delta^{18}O_{atm}$ data in the deeper part of the core do not allow to extend the chronology beyond ~150 ka (gas age) at 1438 m depth. Moreover, the complexity of the glaciological background in the lowermost portion of the TALDICE ice core makes the definition of a preliminary age scale based on the pure glaciological modelling hard to obtain. Indeed, the ice flow dynamics are complex at Talos Dome site. The ice stream surges on the two sides of the dome, either through the small outlets located in the Transantarctic Mountains, or through Wilkes Land, near an efficient ice stream (Masson-Delmotte et al., 2011). The internal layering below the dome is detectable only up to 1400–1500 m. Below that limit reflecting horizons are irregular and discontinuous (Frezzotti et al., 2004). In addition, stratigraphic markers in the deeper portion of the ice core, such as volcanic layers (tephra and sulphates peaks), are not detected below 1400 m depth (Delmonte and Severi, *personal comm.*). To expand the age scale back in time, Bazin et al. (2013) point out that new $\delta^{18}O$ (or δD) and $\delta^{18}O_{atm}$ records at higher resolution are necessary in the deep part of the core, to improve synchronization with other ice core records and to assess the stratigraphic integrity of the ice.

In this work we present the new age scale, named TALDICE-deep1, for the TALDICE ice core between 1438 m and 1548 m depth based on the combination of classical and new dating techniques. We base our chronology on new measurements of gas phase parameters ($\delta^{18}O_{atm}$, $\delta^{15}N$ and $\delta O_2/N_2$) and δD for the ice phase. In addition, considering the complicated glaciological background and the lack of climatic signal below 1548 m depth, we integrate the dating approach with the application of the novel ^{81}Kr dating technique on three different depth intervals. We build the new age scale with the use of the IceChrono1 probabilistic model (Parrenin et al., 2015), which requires the selection of gas markers, ice markers and the definition of a background scenario for the accumulation rate, thinning function and LID. We use a similar strategy to the one employed by Bazin et al. (2013), however we adapt it to the complicated conditions of the deepest portion of TALDICE. In particular, we define gas and ice age markers through the comparison of TALDICE with only EDC $\delta^{18}O_{atm}$ and δD records, avoiding a multicore approach, due to high uncertainties associated with the background scenario. We do not include the CH_4 record in our synchronization strategy since the available data set (Buiron et al., 2011; Schüpbach et al., 2011) below 1438 m depth has not the necessary high resolution needed for comparison with other cores. Moreover, because of the centennial variability of CH_4, this tracer cannot be used to check the integrity of the stratigraphy. In addition to $\delta^{18}O_{atm}$, considering the absence of stratigraphic markers (e.g. volcanic layers) in this portion of the core, we define

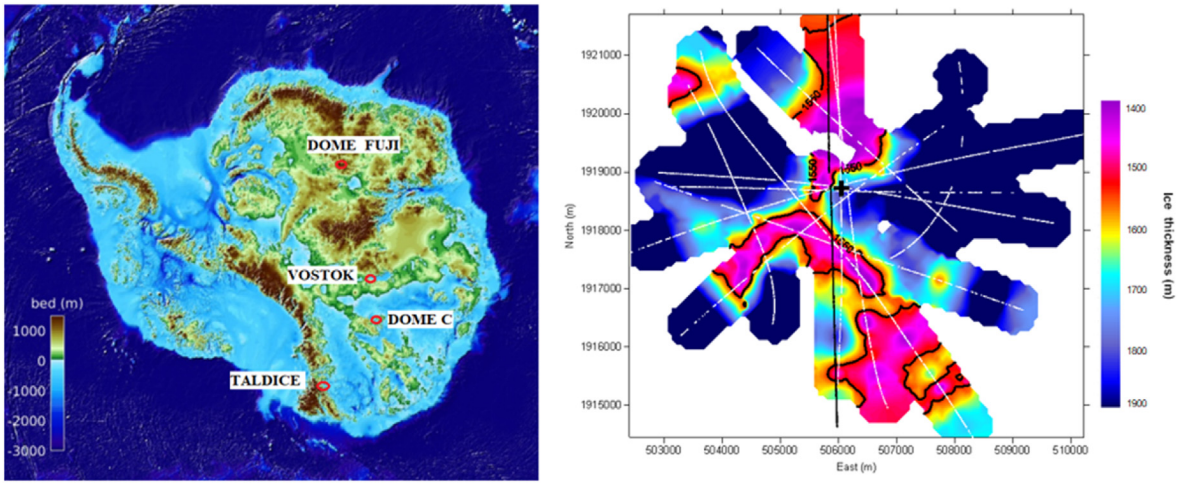

Fig. 1. Location of East Antarctic deep cores on bed topography map (BedMachine) (Morlighem et al., 2020) (a) and radar survey in the Talos Dome area (b). In figure (b) black line indicates depth and contours of subglacial hills and the black cross indicates the TALDICE drilling site (Jordan et al., 2008).

ice markers from water isotopes profiles synchronization.

This paper is structured as follows: we provide new gas and ice data set, as well as ^{81}Kr dating results, from 1438 m to the bottom (section 2), synchronization results (section 3), background chronology definition (section 4) and the inverse method approach to construct the TALDICE-deep1 chronology (section 5). Results, uncertainties and *a posteriori* evaluation of the ^{81}Kr dating method are discussed in section 6, along with a preliminary climatic interpretation of the new δD record.

2. New data set for TALDICE

2.1. $\delta^{18}O_{atm}$, $\delta O_2/N_2$ and $\delta^{15}N$

Buiron et al. (2011) and Bazin et al. (2013) report the isotopic and the elemental composition of trapped air ($\delta^{18}O_{atm}$, $\delta^{15}N$ and $\delta O_2/N_2$) for the TALDICE core in 228 samples between 583 m and 1553 m depth with a mean resolution of 1.5 ka. To increase the resolution of the available data set and to obtain a complete record down to the bottom of the core, 81 new data points are added. Ice samples of ~40 g each, stored at −20 °C, are decontaminated and handled following the procedure described in Extier et al. (2018). The extraction of air trapped in the ice is performed at LSCE, using a semi-automatic extraction line (Capron et al., 2010), and $\delta^{18}O_{atm}$, $\delta^{15}N$ and $\delta O_2/N_2$ of air are measured using a dual inlet Delta V plus (Thermo Electron Corporation) mass spectrometer. To produce the final dataset, several corrections are applied on raw data, taking into account instrumental sensitivity and processes acting in the firn as described in Extier et al. (2018). Lastly, the $\delta^{18}O_{atm}$ record is corrected for gas loss fractionation using $\delta O_2/N_2$ data.

The new $\delta O_2/N_2$ dataset is characterized by low values, i.e. on average - 62 ± 25‰ with values down to −124‰ (Figure 2a and b). The typical values of $\delta O_2/N_2$ for ice analysed shortly after drilling and not affected by gas loss are around −10‰ at Dome C (Extier et al., 2018), and such values were also previously observed at TALDICE (Figure A.1). Due to the gas loss, our new $\delta O_2/N_2$ results cannot be directly used for dating purposes, but they are still useful to correct $\delta^{18}O_{atm}$ data as in previous studies (Extier et al., 2018; Severinghaus et al., 2009). For samples showing $\delta O_2/N_2$ values more negative than −50‰ (i.e. much more negative than values measured before in ice cores affected by gas loss), the equation proposed by Extier et al. (2018) does not correct properly the $\delta^{18}O_{atm}$. We thus propose an alternative gas loss correction equation tailored for samples affected by extreme gas loss, based on EDC $\delta^{18}O_{atm}$ and $\delta O_2/N_2$ data set. Detailed gravitational and gas loss correction calculations are described in Appendix A.

The new $\delta^{18}O_{atm}$ data set fits well with the available profile of TALDICE (Buiron et al., 2011; Bazin et al., 2013), validating our measurements and gas loss correction approach. The extended and corrected $\delta^{18}O_{atm}$ and $\delta O_2/N_2$ datasets between 1350 m depth and the bottom are shown in Figure 2. Due to the small size of the available samples, measurements in replicates are not possible. The 1σ uncertainty associated with the measurements is calculated on 30 replicates of air samples and is equal to ±0.04‰ for the $\delta^{18}O_{atm}$ data set, ± 1.24‰ for $\delta O_2/N_2$ measurements and ±0.02‰ for $\delta^{15}N$ data. The combined $\delta^{15}N$ record is also used to estimate the LID. Detailed explanations and LID calculation are reported in section 4.2.

2.2. ^{81}Kr dating

Krypton is a noble gas present in the atmosphere with a concentration of 1.10 ppmv (Aoki and Makide, 2005). Its ^{81}Kr isotope, with an atmospheric abundance of $9.3 \cdot 10^{-13}$ (Zappala et al., 2020), is naturally produced in the upper atmosphere by cosmic-ray induced spallation and neutron activation of stable krypton (Loosli and Oeschger, 1969; Lu et al., 2014). ^{81}Kr has a long residence time in the atmosphere and, due to its chemical stability, is well-mixed. Buizert et al. (2014) suggests that ^{81}Kr might be applied as a dating tool for ancient air trapped in polar ice, in the 0.03–1.3 Ma age range, also for cores affected by disturbed stratigraphy or discontinuous records.

^{81}Kr dating represents a new dating approach in ice cores. Until now it has been successfully applied only on outcropping old ice from Taylor Glacier, Antarctica (Buizert et al., 2014) and Guliya Ice Cap, Tibetan Plateau (Tian et al., 2019). The typical sample size for the initial study is about 40–80 kg of ice, from which 5–10 μL STP of krypton can be extracted for the analysis with the Atom Trap Trace Analysis (ATTA) method (Jiang et al., 2012; Lu et al., 2014). However, recent developments of the ATTA machine reduces the sample size down to 1 μL STP of krypton, which can now be extracted from about 10 kg of Antarctic ice (Jiang et al., 2020; Tian et al., 2019).

In order to provide an absolute dating of three different depth intervals in the lowermost part of the TALDICE core and to assess the integrity of ice stratigraphy, three samples covering consecutively 4–5 m core length each and weighing from 5.5 to 9.5 kg, are

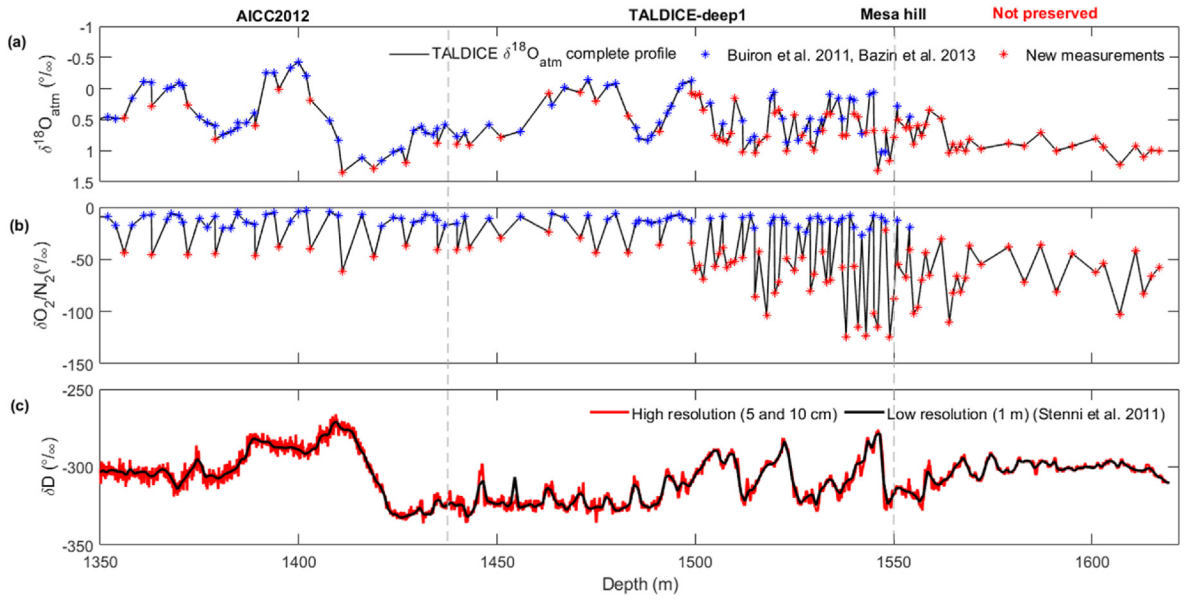

Fig. 2. New data set for deep portion of the TALDICE ice core. $\delta^{18}O_{atm}$ (a) and $\delta O_2/N_2$(b) record between 1350 m and 1620 m depth, new measurements presented in this study (red stars) and measurements published by (Bazin et al., 2013; Buiron et al., 2011) (blue stars). δD record between 1350 m and 1620 m depth (d), the new high resolution δD profile (red curve) (10 cm between 1438 m and 1486 and 5 cm resolution below 1438 m depth to the bottom) is superimposed on 1-m resolution δD record (black curve) (Stenni et al., 2011). The core is divided in three sections on the basis of the chronology. From the top until 1438 m TALDICE is dated by the AICC2012 chronology, between 1438 m depth and 1548 m depth we define the TALDICE-deep1 age scale. Below 1548 m depth the climatic signal is not preserved. The mesa hill is depicted at 1550 m depth. (For interpretation of the references to colour in this figure legend, the reader is referred to the Web version of this article.)

selected between 1560 and 1617 m depth. The chosen samples belong to 13 1-m-long bags of TALDICE CUT B (54 × 55 mm), stored at the European Cold Laboratory Facilities (University of Milano-Bicocca, Italy) at −30 °C. We ship the bags to LSCE (France) with a dedicated transport at constant temperature of −20 °C and then store in the cold room at the same temperature for several weeks. We carry out samples cutting, decontamination and air extraction at LSCE, following the protocol described in Tian et al. (2019). We extract air from TALDICE samples and collected in three stainless steel cylinders that we send to the University of Science and Technology of China (USTC) for krypton purification and ^{81}Kr analysis with the ATTA method, as described by Jiang et al. (2012) and Dong et al. (2019). The anthropogenic ^{85}Kr is measured simultaneously with ^{81}Kr to quantify any contamination with modern air. The ice sample details and krypton dating results are reported in Table 1. For all three samples the measured ^{85}Kr activity is below the detection limit, so no correction for contamination with modern air is necessary. For the calculation of the ^{81}Kr-ages, the changes in the past atmospheric ^{81}Kr abundance due to variation of the cosmic ray flux on the Earth (Zappala et al., 2020) are taken into account. The age uncertainty calculation is based on the statistical error of the atom counting. The detailed ^{81}Kr data analysis can be found in Appendix B.

2.3. δD of water

The complete record of hydrogen isotopic composition (δD) in the TALDICE ice core at 1-m resolution is published in Stenni et al. (2011). The 1-m record is characterized by a resolution of 128 years/m during the LIG, when the AICC2012 chronology ends. Here we present new continuous δD dataset at 5 and 10 cm resolution starting at 1438 m down to the bottom, which aims at increasing the record resolution. Discrete samples at 10 cm-resolution between 1438 m and 1486 m depth are measured at the University of Venice using a Thermo Fisher Delta Plus Advantage mass spectrometer coupled with a HDO device. The precision of δD measurements is ±0.7‰ (1σ). Below 1486 m depth, discrete 5 cm-resolution analyses are carried out the University of Venice and LSCE using the Cavity Ring Down Spectroscopy technique (CRDS). Analysis are performed using a Picarro isotope water analyser (L2130-i version) for both laboratories. The data are calibrated using a linear calibration with three lab-standards periodically calibrated vs V-SMOW. Intercomparison of standard waters are performed between the two laboratories over the analysis period.

A comparison of our new δD TALDICE record with the previous data set published by Stenni et al. (2011) is shown on Figure 2c.

Table 1
Ice sample details and radio krypton dating results. Reported errors are 1-σ errors. Upper limits have a 90% confidence level. The average ^{85}Kr activity in the northern hemisphere has been ~75dpm/cc at the time of sample processing. The measured ^{85}Kr concentrations are below the detection limit, verifying that no relevant contamination with modern air has occurred. Additional to the statistical error on the ^{81}Kr-age from atom counting, a systematic error due to the uncertainty in the half-life of ^{81}Kr has to be taken into account. This error would shift all ^{81}Kr ages up or down together. [a] dpm/cc = decay per minute/cubic centimetre STP of krypton, [b] pMKr = percent modern Krypton.

Depth (m)	Air Extracted/Ice Weight (mL STP/kg)	Sample Used (μL STP, Kr)	^{85}Kr (dpm/cc)[a]	^{81}Kr (pMKr)[b]	^{81}Kr-Age (ka)	Systematic error (ka)
1559–1563	700/9.6	~0.7	<0.3	30.5 ± 1.6	397 ± 18	±19
1573–1575	550/5.4	~0.6	<0.8	24.9 ± 3.5	470 ± 54	±23
1577–1578						
1613–1618	760/9.5	~0.8	<0.1	29.4 ± 1.5	410 ± 19	±20

3. Synchronization and age markers definition

Ice flow modelling for dating the ice, as well as the identification of dated volcanic horizons (e.g. tephra layers, sulphate spikes) and orbital tie points represent the main classical strategies to define the ice chronology. The deep part of TALDICE ice core, unfortunately, does not provide suitable conditions to employ any of the above mentioned approaches. We decide to apply a dating strategy which involves the use of the new $\delta^{18}O_{atm}$ TALDICE profile as a stratigraphic tool, synchronizing it with the dated EDC signal (Extier et al., 2018) in parallel with the alignment between TALDICE and EDC δD signals (EPICA Community Members, 2004). The synchronization between δD records is based on the principle that large climatic variations observed in the stable water isotopes records are synchronous in all Antarctic cores. The δD matching becomes an essential tool, in our case, to find the best visual matching scenario and to provide markers to define the ice age scale.

3.1. $\delta^{18}O_{atm}$ synchronization

The new TALDICE $\delta^{18}O_{atm}$ profile allows the synchronization of the record below 1438 m depth with the extended $\delta^{18}O_{atm}$ data set published for the EDC ice core (Extier et al., 2018) on the AICC2012 gas age scale (Bazin et al., 2013). We select the EDC dataset spanning the time window from Termination III to Termination IV at relatively high resolution: ~160 years for Termination III and ~700 years for Termination IV (Extier et al., 2018). Due to the relatively low resolution of our TALDICE $\delta^{18}O_{atm}$ record (1.55 m, ~2620 years), we cannot apply any automatic matching algorithm for synchronization. We employ the manual wiggle-matching technique to choose TALDICE tie points. When possible, we define tie points at mid-slope, however maxima and minima are selected as well. We perform several sensitivity tests increasing and decreasing the number of tie points and verifying the degree of agreement between the two records. After several visual experiments we define 22 gas age markers between 1455.92 m and 1548 m depth (Table 2), which represent the minimum number of data points allowing superimposition of the two curves with the maximum degree of agreement ($r = 0.81$) (Figure 3). Within these 22 tie points, 15 are located at slope breaks (50%, 25% or 75% of the transition) in the TALDICE record, 6 points at maxima and 1 at a minimum.

Then, we associate with each tie point a corresponding AICC2012 age from the EDC $\delta^{18}O_{atm}$ record(Figure 3a). The final age of each TALDICE tie point is calculated as the mean age obtained from five different possible visual matchings between the two records, following a similar approach applied by Capron et al. (2010). The uncertainty (reported in Table 2) is calculated adding the uncertainty of the visual matching between TALDICE and EDC $\delta^{18}O_{atm}$ records (difference between the maximum and the minimum estimated EDC AICC2012 age for one single TALDICE tie point), TALDICE $\delta^{18}O_{atm}$ resolution on the initial TADICE-1 age scale (Buiron et al., 2011) and the uncertainty associated with AICC2012 gas age scale for EDC. Detailed uncertainty calculations are reported in Appendix C. As expected, the synchronization results show a good agreement between the two $\delta^{18}O_{atm}$ records in the time span 158–252 ka ($r = 0.86$), the TALDICE record displays a signal similar to the EDC one in terms of shape and intensity. On the other hand, between 252 and 280 ka the matching between the two profiles appears less clear ($r = 0.60$) due to the relative higher values of the TALDICE $\delta^{18}O_{atm}$ record (average of ~0.70‰) with respect to the EDC ones (average of ~0.48‰), and the lack of the ~260 ka peak in our data set, attributable to the low resolution. For the part older than 280 ka, a good agreement ($r = 0.62$) between the two data set is visible until Termination IV (~343 ka). In order to refine the synchronization during this time period we perform 7 new $\delta^{18}O_{atm}$ measurements on the EDC core in the time interval between 335 ka and 337 ka (2587.20–2594.90 m depth), which improves the resolution over the ~336 ka excursion just at the start of the deglaciation (Figure 3b). This short event is also visible in the TALDICE profile, and it allows the synchronization of the two records with a high degree of confidence until 335 ka. Below 1548 m depth, corresponding to a gas age of 336 ka, the synchronization is more difficult due to the lower variability of $\delta^{18}O_{atm}$ and we do not select additional tie points (Figure 3a).

The uncertainty associated with the $\delta^{18}O_{atm}$ records synchronization spans from a minimum of 2.7 ka to a maximum of 7.9 ka, and its evolution along with the depth is variable and strictly influenced by the uneven sampling of TALDICE $\delta^{18}O_{atm}$ data points (see Table 2). However, our simple synchronization provides a uniform evolution of the gas age scale as a function of depth and allows for identification of a preserved $\delta^{18}O_{atm}$ signal down to 1548 m depth.

Table 2
Tie points defined by $\delta^{18}O_{atm}$ record synchronization between TALDICE and EDC ice cores on the AICC2012 gas age scale.

Depth TALDICE (m)	Depth EDC (m)	Gas age (ka)	Uncertainty (±ka)
1447.92	1930.08	158.8	4.9
1455.92	1919.42	163.1	4.3
1483.00	1991.81	179.8	4.0
1492.95	2041.79	190.3	6.2
1498.95	2068.01	195.7	5.8
1503.87	2089.34	199.7	2.7
1509.00	2143.21	209.3	5.0
1510.00	2181.61	215.9	7.7
1511.92	2221.86	224.0	5.4
1518.00	2256.98	233.7	6.5
1519.90	2284.32	239.7	3.7
1521.93	2298.62	242.2	3.0
1525.00	2331.01	248.7	3.9
1527.95	2352.46	256.6	5.2
1528.92	2364.23	261.0	7.9
1529.00	2391.71	270.6	7.7
1533.00	2426.71	282.9	3.8
1536.93	2460.24	293.2	5.4
1538.92	2500.29	308.1	4.6
1541.00	2513.95	314.0	6.8
1545.00	2580.40	334.4	3.5
1548.00	2589.72	336.3	3.0

3.2. Water isotopes synchronization

We define ice age markers through the synchronization between the new TALDICE δD profile below 1438 m depth and the EDC δD profile (55 cm resolution) (EPICA community members, 2004) drawn on AICC2012 ice age scale, which covers the last 800 ka (Bazin et al., 2013). For matching purposes, we select the EDC δD portion of the profile spanning from 150 ka to 450 ka, with a mean data resolution of ~250 years for Termination III and ~340 years for Termination IV. The preliminary estimation of the temporal resolution of TALDICE water isotopes below 1438 m depth, obtained from the δD synchronization, is ~127 years for Termination III and ~190 years for Termination IV. We employ the same visual synchronization approach applied for the $\delta^{18}O_{atm}$ record, but here we mainly select mid-slopes points thanks to the high-resolution of both EDC and TALDICE records.

The choice of tie points has fallen on the minimum number of points (18), which provides the highest degree of agreement between the two records ($r = 0.91$), with the purpose of better constraining the synchronization over the interglacial periods MIS 7.5 and 9.3. The result of the δD visual matchings are displayed in Figure 4. The complete list of the selected tie points and the

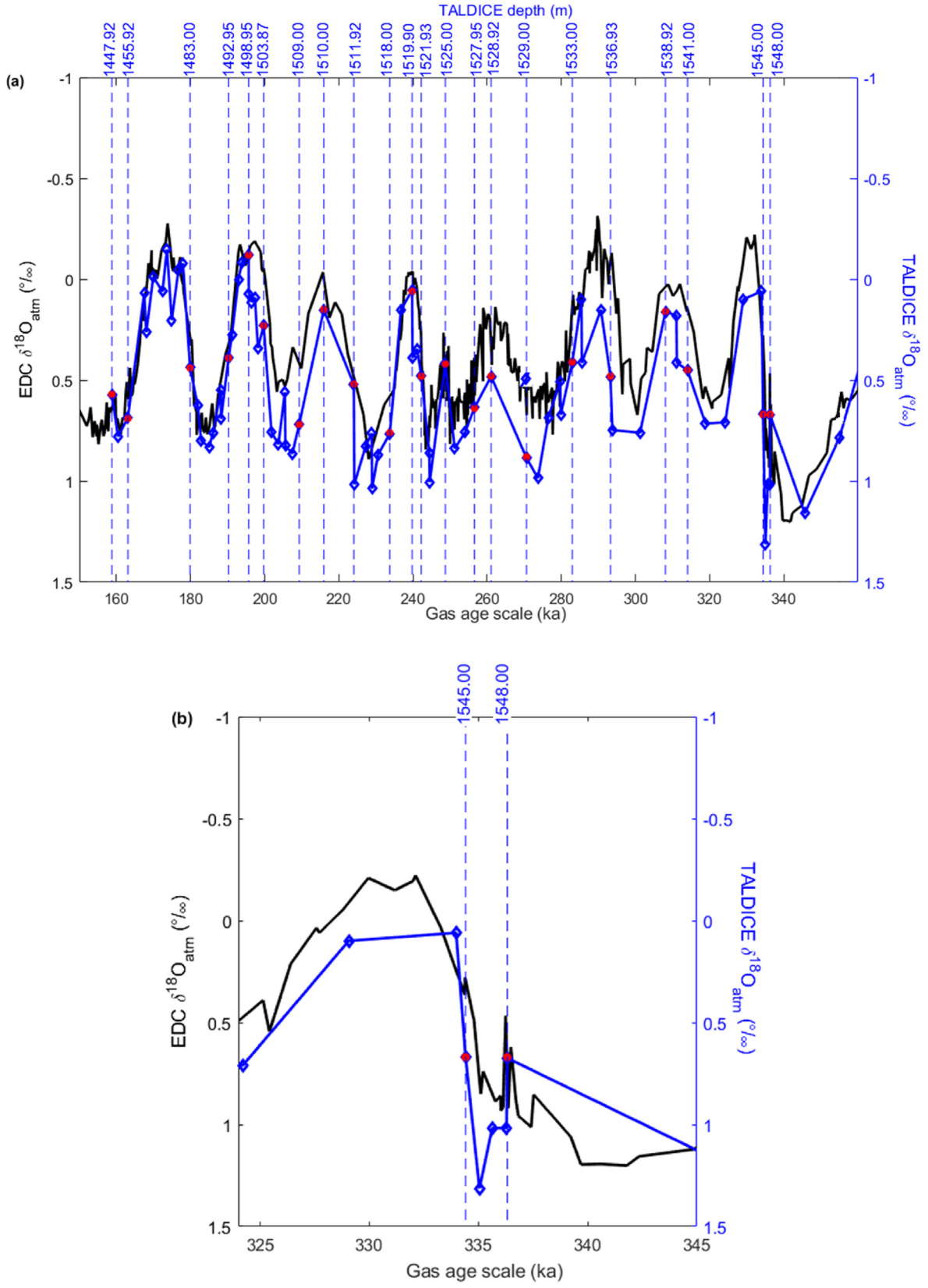

Fig. 3. Synchronization of TALDICE and EDC $\delta^{18}O_{atm}$ records between 150 and 336 ka. (a) TALDICE (blue curves) $\delta^{18}O_{atm}$ record and gas tie points (red dots) synchronized on EDC (black curve) (Extier et al., 2018 and new measurements) drawn on the AICC2012 gas age timescale (Bazin et al., 2013) (b). Focus on new event detected before Termination IV in both cores. (For interpretation of the references to colour in this figure legend, the reader is referred to the Web version of this article.)

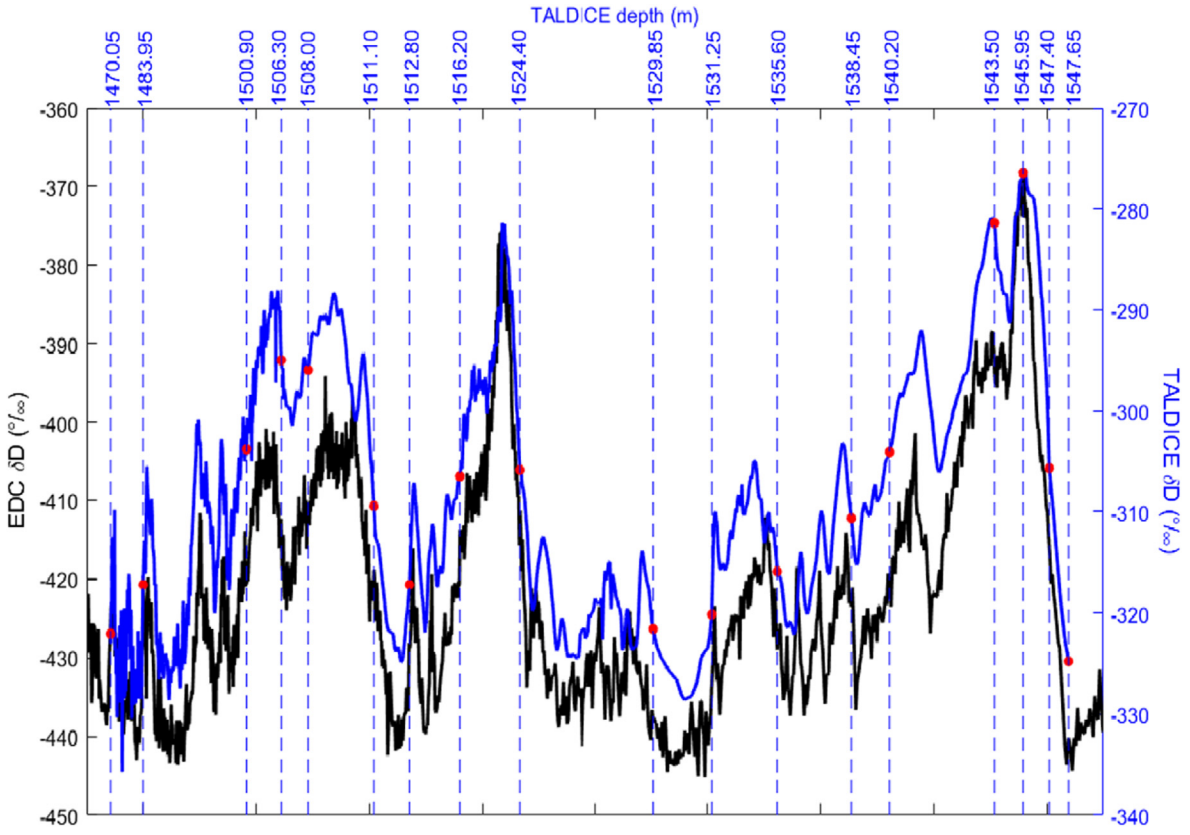

Fig. 4. Synchronization of TALDICE and EDC δD records between 150 and 350 ka. TALDICE (blue curves) δD record and ice tie points (red dots) synchronized on EDC (black curve) (EPICA community members, 2004) drawn on the AICC 2012 ice age timescale (Bazin et al., 2013). (For interpretation of the references to colour in this figure legend, the reader is referred to the Web version of this article.)

associated uncertainties are reported in Table 3. Each marker point has an associated uncertainty, called cumulative uncertainty, and its calculation is explained in details in Appendix C. The synchronization effort exhibits a good agreement between the two isotope profiles between ~174 and ~249 ka (r = 0.88), as during MIS 7 substages are well constrained. The uncertainties of the tie points in this age window are almost constant and set around the average value of ~3.5 ka. In contrast, the portion older than ~249 ka, is characterized by larger uncertainties up to 6 ka when constraining the MIS 9, since the TALDICE isotope profile show a second interglacial peak around ~330 ka which is not identified in the EDC δD signal (more details are given in section 6.3). However, the synchronization provides a high degree of agreement (r = 0.95) between the two records down to the depth of 1547.65 m, where the estimated ice age is ~343 ka. Below 1548 m depth we cannot observe any similarity between TALDICE and EDC δD records, concluding that no climatic signal is preserved in this portion of the core. The δD signal below the last tie point does not show any significant variability, similarly to what is observed in the $\delta^{18}O_{atm}$ profile (Figure 3).

Table 3
Tie points defined by δD record synchronization between TALDICE and EDC ice cores on the AICC2012 ice age scale.

Depth TALDICE (m)	Depth EDC (m)	Ice age (ka)	Uncertainty (ka)
1470.05	1951.07	174.2	3.0
1483.95	1976.48	180.0	2.7
1500.90	2065.91	198.3	3.6
1506.30	2102.32	204.4	2.6
1508.00	2125.53	209.2	4.0
1511.10	2196.59	220.8	3.9
1512.80	2220.68	227.1	3.5
1516.20	2253.90	236.0	3.7
1524.40	2312.42	246.6	3.1
1529.85	2381.50	270.4	5.8
1531.25	2410.21	280.7	2.9
1535.60	2448.49	292.3	3.5
1538.45	2486.11	305.4	3.0
1540.20	2502.06	312.2	6.3
1543.50	2556.84	330.7	5.3
1545.95	2579.17	335.8	3.4
1547.40	2595.56	340.4	4.4
1547.65	2602.60	343.8	3.2

4. Background scenario

To build the TALDICE-deep1 age scale we employ the inverse model IceChrono1 (Parrenin et al., 2015), which provides the best compromise between a background chronology (based on ice flows and snow densification simulations) and observations (ice and gas stratigraphic links between cores and absolute ages). The background scenario is defined by three profiles in function of depth for the following glaciological parameters: thinning function, accumulation rate and LID. The background scenario is usually computed by firn densification and ice flow models; however, the LID can be calculated from the application of the firnification model as well as from the barometric equation using $\delta^{15}N$ data. In the following two sub-sections we describe how we define the background scenario associated with the deep portion of the TALDICE ice core, integrating previous estimation of glaciological parameters from Buiron et al. (2011) (Section 4.1) with our new $\delta^{15}N$ data set (Section 4.2).

4.1. Accumulation rate and thinning function

In order to build the TALDICE-deep1 age scale we use the accumulation rate and thinning function estimated by Buiron et al. (2011) for the TALDICE-1 age scale until 1597 m depth, while we estimate a new LID profile from novel $\delta^{15}N$ measurements (Section 4.2). Our choice is driven by the fact that no new data set of field measurements is available for the TALDICE ice core for the accumulation rate and the thinning function, estimated with the 1-D ice flow model (Parrenin et al., 2007).

Input parameters for the 1-D model are past accumulation rate and temperature changes. Those quantities are derived from the hydrogen isotopic content of the ice (δD) through the following equations:

$$T = T^0 + \Delta\delta D_{corr}\alpha \quad (1)$$

$$A = A^0 \exp\left(\beta\Delta\delta Ds_{mo}\right) \quad (2)$$

where T^0 and A^0 are the current surface temperature (°C) and accumulation rate (cm of ice equivalent per year) at the ice core site. $\Delta\delta D_{corr}$ is the temporal deviation to the present-day hydrogen isotopic content of precipitation at the site, corrected for past $\delta^{18}O_{sw}$ variations derived from the marine benthic stacks (Lisiecki and Raymo, 2005). Due to the lack of the complete TALDICE δD profile, Buiron et al. (2011) calculate the record multiplying by 8 the available $\delta^{18}O$ data set (Stenni et al., 2011). We decide to use the Buiron et al. (2011) data set as well, even if the 5 and 10 cm δD profile is now available, as it would not impact on the background scenario. $\Delta\delta D_{smo}$ is a 50-yr average of $\Delta\delta D_{corr}$, α represents the spatial slope present-day isotopic thermometer (Frezzotti et al., 2004; Magand et al., 2004) and β is related to the glacial-interglacial amplitude of accumulation rate changes, tuned for the best fit of age markers for the TALDICE-1 chronology (Buiron et al., 2011). All the coefficients applied in the 1-D model are reported in Buiron et al. (2011). Unfortunately, the model contains poorly-constrained parameters and a simplistic description of the ice flow, generating errors in the estimation of the thinning function and accumulation rate profile with respect to the depth, especially in the lowermost portion of the core (below 1500 m depth). For such reason, we define high relative uncertainties as constant values and larger with respect to the pure values of thinning function and accumulation rate, respectively equal to $\sigma = 1$ and $\sigma = 0.5$.

4.2. LID estimation from the new $\delta^{15}N$ data set

The LID can be estimated either from firnification model (Goujon et al., 2003) or from the isotopic composition ($\delta^{15}N$) of gases trapped in the ice (Landais et al., 2006).

Taking into account the firn density increase from the surface to the depth where air stops diffusing, the firnification model defines the LID as:

$$LID = \int_0^{LID} D(y,t)dy \quad (3)$$

where D is the density of the material at the time t and at vertical coordinate y (Parrenin et al., 2012).

The LID (m) can also be estimated independently from the firnification model, and based on the $\delta^{15}N$ profile, through the application of the barometric equation (Sowers et al., 1992):

$$\delta^{15}N = \Delta mgLID \Big/ RT \quad (4)$$

where Δm is the mass difference between ^{15}N and ^{14}N ($gmol^{-1}$), g is the gravitational acceleration (ms^{-2}), R the gas constant ($JK^{-1}mol^{-1}$) and T the mean firn temperature (K). T is calculated following equation (1) reported in section 4.1. The Lock-in-Depth in Ice Equivalent (LIDIE) is then calculated multiplying the LID by 0.7, the compaction factor typical of modern conditions on the East Antarctic Plateau (Herron and Langway, 1980; Parrenin et al., 2012), as no firn density profile is available for the deeper portion of TALDICE. For the definition of TALDICE-1 age scale, Buiron et al. (2011) estimate the LIDIE until 1597 m depth through the application of the firnification model. Here, we calculate the LIDIE profile for the portion of the core between 1356 and 1597 m depth from our new $\delta^{15}N$ data set for the definition of the TALDICE-deep1 chronology.

The uncertainty associated with our $\delta^{15}N$-LIDIE estimation is described in Appendix C. In Figure 5, we compare the two LIDIE estimations and we observe that the firnification model estimates a quasi-constant LIDIE of ~62 m over the depth range of interest (1438−1597 m depth), while the LIDIE deduced from the $\delta^{15}N$ data set (smoothed red curve, Figure 5a) shows an increasing trend with depth, from ~48 m at 1438 m depth to ~65 m at 1597 m depth. We also calculate the difference between the two estimated quantities (Figure 5b) and we find out that it decreases over depth. At 1438 m the LIDIE calculated with the firnification model exceeds the LIDIE obtained from the barometric equation by ~16 m, while at ~1574 m depth the two parameters converge on the common value of ~60 m. Below that depth, down to 1597 m, the LIDIE deduced from $\delta^{15}N$ data becomes larger of about 5 m with respect to the modelled one.

5. TALDICE-deep1 age scale based on a probabilistic model

IceChrono1 is an inverse model based on a similar approach to the Datice tool (Lemieux-Dudon et al., 2010), which is used to build both the TALDICE-1 age scale (Buiron et al., 2011) and the TALDICE AICC2012 age scale (Bazin et al., 2013), but including mathematical, numerical and programming improvements. The dating strategy of IceChrono1 is based on finding the best compromise between the background scenario and observations (absolute ages, stratigraphic links between cores, orbital ages and reference horizons) of several cores. It combines different sources of information, mathematically described as probability density functions (PDF), which are supposed to be independent (prior and observation) and are combined using a Bayesian framework to obtain the most probable scenario. This scenario provides *a posteriori* estimation of the background parameters and the ice and gas chronologies (Parrenin et al., 2015).

To construct the TALDICE-deep1 chronology we adopt a simplified approach, avoiding the multi-cores comparison strategy as in IceChrono1, and synchronize the TALDICE ice and gas records only with the EDC core data. Below 1438 m depth the background scenario (thinning function and the accumulation rate parameters) is poorly constrained and the multi-core synchronization effort would not improve the age scale quality. We use the following parameters as input files for IceChrono1 model: (i) the background scenario, which consists in accumulation rate, thinning function and LIDIE quantities defined with respect to depth (as described in section 4); (ii) gas stratigraphic links (tie points) between TALDICE and EDC $\delta^{18}O_{atm}$ profiles (section 3.1); (iii) ice stratigraphic links (tie points) between TALDICE and EDC δD signals (section 3.3); (iv) absolute ages obtained from ^{81}Kr dating, with the exception of the bottom sample (section 3.4). In addition, we define the relative uncertainties associated with all the elements of the background

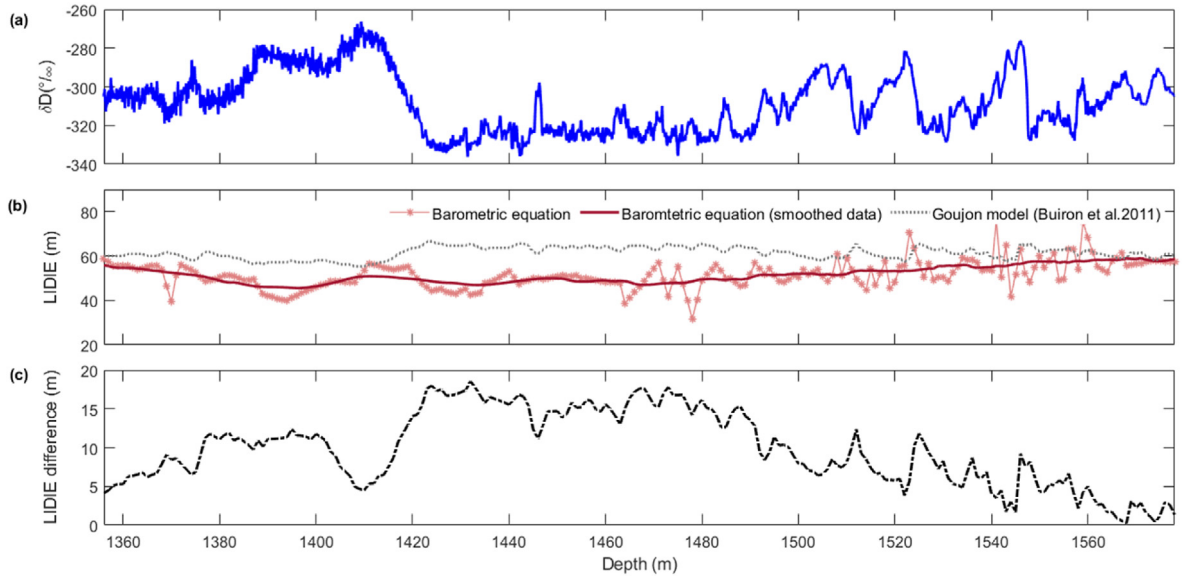

Fig. 5. LIDIE for the deep portion of the TALDICE ice core. New δD profile (‰) (a). LIDIE estimated with the Goujon model (grey curve) applied for the TALDICE-1 age scale (Buiron et al., 2011) and LIDIE calculated from barometric equation with our new $\delta^{15}N$ data set (dark red curve with star markers) and smoothed data (red curve) (b), both profiles are function of depth. Difference between LIDIE defined from firnification model and the LIDIE calculated from the barometric equation (m) in function of depth (c). (For interpretation of the references to colour in this figure legend, the reader is referred to the Web version of this article.)

scenario and the cumulative uncertainties related to gas and ice tie points. Uncertainties are carefully estimated and calculations are detailed in Appendix C. All the input files are defined until 1578 m depth, which corresponds to the last ^{81}Kr age that we consider to be coherent with our gas synchronization results.

6. Results and discussion

6.1. The TALDICE-deep1 age scale and added value of ^{81}Kr dating results

The combination of our different observations for the portion of the TALDICE ice core below 1438 m depth (absolute ages, gas stratigraphic links and ice stratigraphic links) with the previous data sets published by Buiron et al. (2011) and Bazin et al. (2013) extends the core chronology beyond the limits set by the AICC2012 age scale. The TALDICE-deep1 gas and ice age-depth relationships, defined from our background scenario on which we applied the inverse model IceChrono1, are shown in Figure 6a and b. In particular, the TALDICE-deep1 age scale exhibits a double-feature evolution as the trend appears coherent with the AICC2012 curve until ~1500 m depth, while below this depth we observe a change in behaviour and the curve shows an extremely steep shape, indicating the presence of enhanced thinning until 1550 m depth.

The inverse model also calculates the chronology uncertainty in the chronology, which is influenced by the errors associated with tie points and dated horizons. Figure 6c shows the uncertainty related to the age-scale at different ages. The youngest portion of the chronology, from ~150 ka to 170 ka, shows a relatively high error of about ~4 ka. This result is influenced by the uncertainty defined over the oldest portion of the AICC2012 age scale, around 150 ka, and the presence of a limited number of markers for both ice and gas matrices. Then, the uncertainty decreases down to an average value of ~2 ka between 170 and 343 ka due to the large number of both ice and gas tie points, which improves the constraints on the chronology.

This study includes the first application of ^{81}Kr analysis on small ice samples (<10 kg) as a tool to assist an ice core chronology. Previous applications of ^{81}Kr dating are performed on 40–80 kg of ice blocks or shallow cores from margin sites. In this application, we date three layers below 1548 m depth to assess the preservation of the stratigraphic order. Indeed, the first ^{81}Kr dated sample is located between 1559 and 1563 m depth and provides an absolute ^{81}Kr age estimation of 397 ± 19 ka. The age depth relationship evolution below 1564 m is driven by the ^{81}Kr dated horizon between at 1573–1578 m, 470 ± 54 ka and the error curve exhibits a sharp increase caused by the high uncertainty associated the two shallower Kr dated layers (Figure 6c). The deepest ^{81}Kr age constraint at 1613–1618 m depth carries a comparable age (410 ± 20 ka) with respect to the upper samples; indicating the presence of processes that induces an alteration of the stratigraphic order, as folding and/or mixing. This finding indicates that ^{81}Kr dating can be applied to date deep ice when no other constraints are available to verify the preservation of the stratigraphy.

We stop the TALDICE-deep1 chronology at 1548 m depth, corresponding to an age of 343 ka. This choice is driven by the absence of climatic variability in the δD and $\delta^{18}O_{atm}$ profiles below this depth and the exponential increase of the age scale uncertainty (Figure 6). In addition, the ^{81}Kr results indicate that below 1548 m depth the stratigraphic order might be compromised. We suggest that the position of the drilling site, located inside a deep gorge and close to a mesa hill at 1550 m depth (Urbini et al., 2008) might cause disturbances of the ice flow and/or folding of the ice at deeper depths or act as holder for stagnant ice (Lilien et al., 2021).

6.2. A posteriori evaluation of the thinning function

The thinning function presented here for the core portion below 1438 m, relies on ice, gas markers and comparison with the EDC timescale because glaciological constraints are not available. Interestingly, (Montagnat et al., 2012) observe that grains with orientations departing from the single maximum appear below ~1410 m down to 1500 m depth hence suggesting a complex glaciological behaviour. Below a depth of 1500 m the increase of crystals size does not allow any statistical analysis (Montagnat,

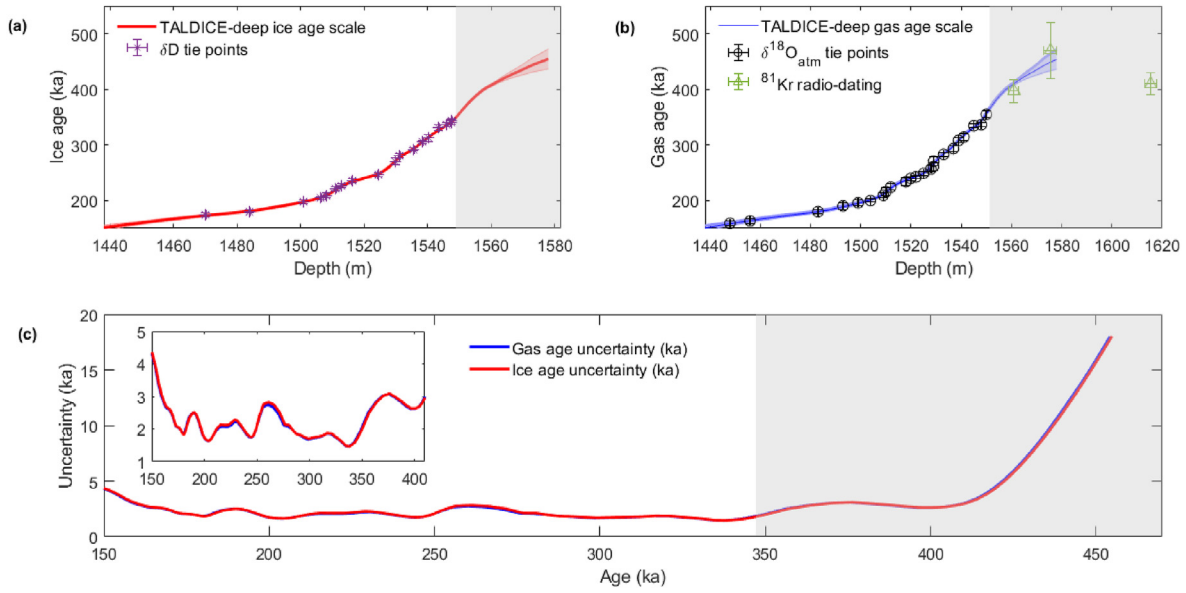

Fig. 6. TALDICE-deep1 age scale for both gas and ice matrix with the respective uncertainties. TALDICE–deep age/depth relationship for the ice matrix (a) and for the gas matrix (b) superimposed on their respective age markers obtained from the synchronization between TALDICE and EPICA δD and $\delta^{18}O_{atm}$ profiles and ^{81}Kr dated horizons (green triangles). Uncertainty in ka associated to the TALDICE-deep1 ice (red curve) and gas (blue curve) chronology (c). The chronology stops at 1548 m depth (343 ka), below that depth we cannot extend the age scale (shaded area). (For interpretation of the references to colour in this figure legend, the reader is referred to the Web version of this article.)

personal comm).

Due to the poor glaciological constraints, we associate the background thinning function defined by Buiron et al. (2011) for the TALDICE-1 age scale with high uncertainties ($\sigma = 1$) to let the ice and gas markers shaping the final thinning function. As shown in Figure 7a, the inverse method computes a thinning function for the deep portion of the ice core which does not agree with the respective *a priori* estimation. The *a posteriori* thinning function is characterized, as the curve defined by the AICC2012 chronology, by the presence of "bumps". These "bumps" are generally the expression of upstream or temporal variations of ice thickness at the deposition site (Parrenin et al., 2004, Parrenin et al., 2007). The TALDICE-deep1 thinning function shows only one bump, visible at 1473 m depth (~175 ka), associated with a value of 0.04, and followed by a sharp decrease in the function down to a value of ~0.01 until 1510 m depth (~220 ka). Considering the large deviation of the *a priori* thinning function from the calculated one (factor of 2) and the complex glaciological background in the deeper portion of TALDICE, this bump can be interpreted as the manifestation of irregular ice flow in those deep layers as observed in the EDC ice core at 500 m from the bottom (Dreyfus et al., 2007). Between 1510 m and 1551 m depth the function shows a quasi-constant

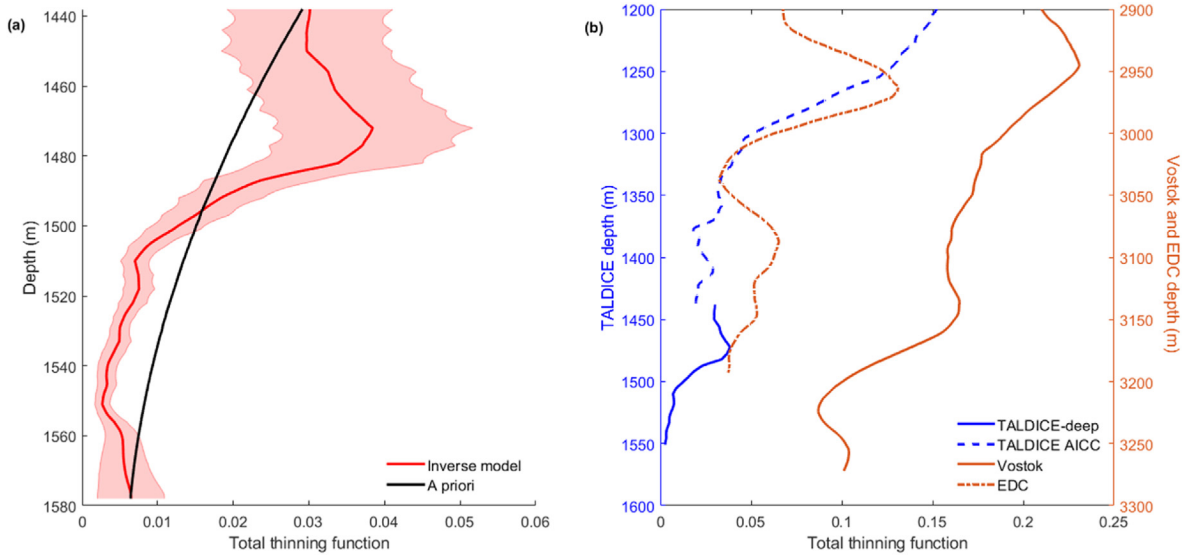

Fig. 7. Thinning functions for TALDICE, Vostok, and EDC. Comparison between the thinning function obtained from the *a priori* ice flow model (black curve) and the one calculated by the inverse model (red line) with the associated uncertainty (red shade) for the deep portion of TALDICE ice core (a). Total thinning functions deduced from the inverse method for Vostok (red curve) and EDC (red dashed curve) (Bazin et al., 2013) and the composite thinning for TALDICE core derived from the inverse model applied to construct the AICC2012 age scale (blue dashed curve) (Bazin et al., 2013) and TALDICE-deep1 chronology versus depth (m) (b). (For interpretation of the references to colour in this figure legend, the reader is referred to the Web version of this article.)

behaviour set on the value of 0.005; while between 1551 m and 1578 m the thinning function tends to join the *a priori* curve as only few constraints (age markers) are defined (Bazin et al., 2013) (Figure 7b). In particular, it is characterized by a steep slope below ~1100 m, as it reaches small values at relatively shallow depths. Similar small values are observed in the Dome Fuji core and are connected to very small basal melting rate (Parrenin et al., 2007). EDC shows a similar behaviour to the TALDICE thinning function, with a "bump" close to the bottom and a *quasi-vertical* shape in the deepest portion of the core. However, for the lowermost portion of the core the thinning function shows values close to 0.05, which are associated with basal melting (Parrenin et al., 2007). On the other hand, the Vostok core shows higher value of the thinning function in comparison to the other cores, close to 0.1 at the bottom. Such different feature at Vostok might be connected to the presence of melting conditions at the bottom due to the influence of the subglacial lake (Parrenin et al., 2004).

The small thinning value below 1500 m indicates that, compared to the other Antarctic cores, TALDICE does not experience melting. The absence of melting processes is also confirmed by the modelled temperature profile with the depth, as the average temperature at the bottom is estimated to be −6 °C (Frezzotti, *unpublished data.*).

6.3. TALDICE δD unique behaviour during interglacial periods

The TALDICE-deep1 age scale extends the core chronology beyond the previous AICC2012 age scale (~150 ka, 1438 m depth) (Bazin et al., 2013) up to ~343 ka (at 1548 m depth). In addition, taking into account the peripheral and coastal position of Talos Dome (Frezzotti et al., 2004), the TALDICE ice core provides the unique chance to investigate the past climate and environmental changes in the Ross Sea sector spanning the last three glacial/interglacial cycles.

Our new δD profile drawn on the TALDICE-deep1 age scale makes possible to identify a well preserved climatic record and to study glacial and interglacial main events and sub-events back to MIS 10.1 (1548 m, ~343 ka) (Figure 8a), which are not identified in other studies (Stenni et al., 2011). The $\delta^{18}O_{atm}$ signal appears as well to be preserved until Termination IV (Figure 8b).

Masson-Delmotte et al. (2011) identify TALDICE as an outlier, in comparison to the other plateau sites, as it shows a different behaviour of the isotopic profile during the LIG at ~118 ka, prior to the glacial inception. Our aim is to study if the TALDICE δD signal shows the same unique behaviour for the older warm periods. We thus perform the same comparison exercise for the oldest interglacial periods MIS 7.5 (240.8–245.8 ka) and 9.3 (324.6–338.8 ka) with Vostok, EDC and Dome Fuji δD records (EPICA community members, 2004; Petit et al., 1999; Uemura et al., 2018) on AICC2012 age scale (Bazin et al., 2013) (Figure 9).

The TALDICE signal is coherent with the Vostok, EDC and Dome Fuji profiles during the culmination of the deglaciation for both MIS 7.5 (~243 ka) and 9.3 (~335 ka), showing a clear shaped peak. On the other hand, prior to the glacial inception, the TALDICE δD curve does not display a monotonous decrease as in the other cores but is characterized by a plateau between 235 and 240 ka for MIS 7.5 and by a second peak during MIS 9.3 (~335 ka) as for MIS 5.5.

Our results confirm that TALDICE appears to record a different climatic and/or environmental signal during interglacials of the past 350 ka in comparison to the other cores drilled in the Antarctic Plateau. Masson-Delmotte et al. (2011) hypothesize that the peculiar behaviour of the water isotopes signal during MIS 5.5 in TALDICE might be connected to elevation changes and/or variations of sea ice extent or changes in the regional high latitude moisture transport. On the other hand, Bradley et al. (2012) explain the same anomaly in the δD signal observed during MIS 5.5 as consequence of a fall in surface elevation along the eastern edge of the Ross Sea over this period. Considering the unique position of the Talos Dome site, located close to the Ross Sea and at the border between the Transantarctic Mountains and Wilkes Subglacial Basin, all hypotheses appear intriguing and further investigation is needed.

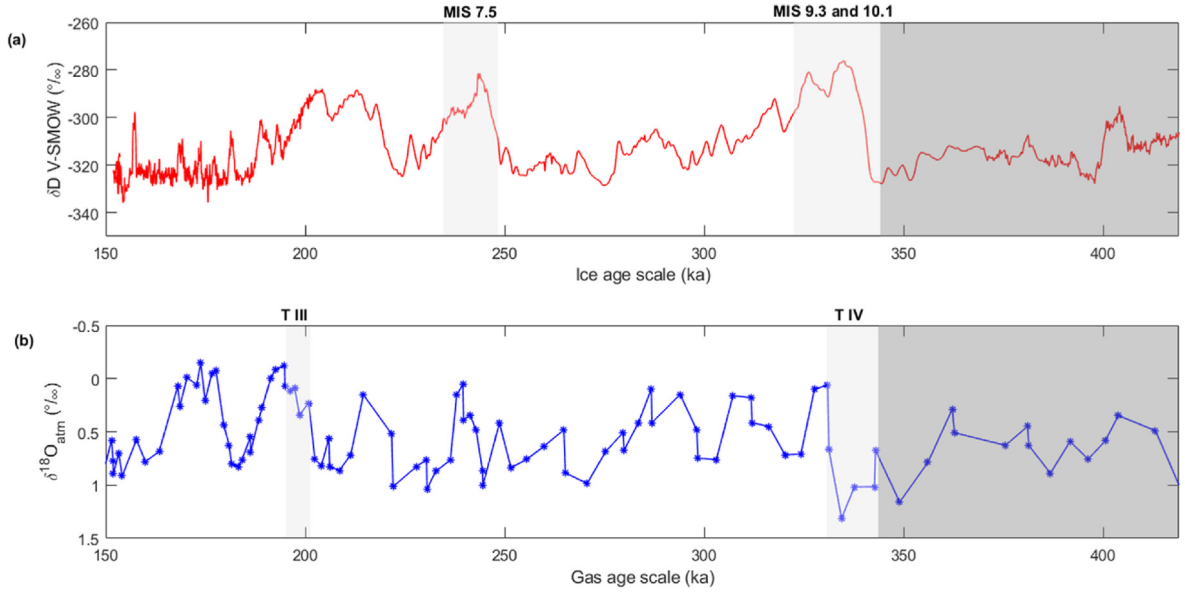

Fig. 8. New δD and $\delta^{18}O_{atm}$ data set on the TALDICE deep-age scale. New δD record of TALDICE ice core on the TALDICE-deep1 age scale (red curve) for the last 343 ka (a). Warm stages 7.5 and 9.3 are highlighted (light grey shading). while the isotopic signal is not preserved on the oldest portion of the core (dark grey shaded area). New $\delta^{18}O_{atm}$ profile (blue curve with stars) on the TALDICE-deep1 chronology (b). Termination III and IV are highlighted (light grey shading). The isotopic signal (δD and $\delta^{18}O_{atm}$) is not preserved below 1548 m depth (dark grey shaded area). (For interpretation of the references to colour in this figure legend, the reader is referred to the Web version of this article.)

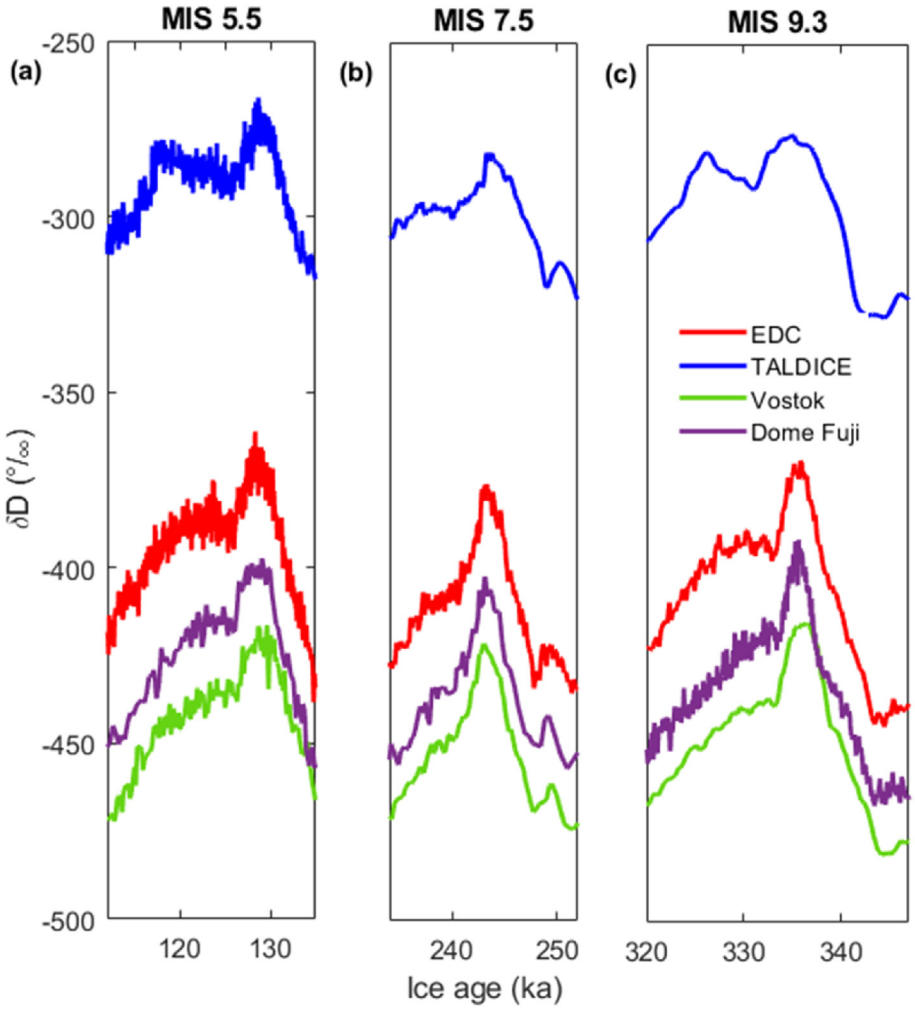

Fig. 9. Comparison of TALDICE water stable isotope record (δD) on AICC2012 (MIS 5.5.) and TALDICE-deep1 (MIS7.5 and 9.3) age scale with other deep Antarctic ice core records. TALDICE δD profile (blue curve) is compared with EDC (red curve), Vostok (green curve) and Dome Fuji ice (purple curve) cores during MIS 5.5 (a), MI 7.5 (b) and MIS 9.3 (b). TALDICE MIS 5.5 (Masson-Delmotte et al., 2011), EDC (EPICA community members, 2004), Vostok (Petit et al., 1999) and Dome Fuji (Uemura et al., 2018) profiles are drawn on the AICC2012 age scale (Bazin et al., 2013). (For interpretation of the references to colour in this figure legend, the reader is referred to the Web version of this article.)

7. Conclusions

In this study we define the chronology called TALDICE-deep1 - for the lowermost and less investigated portion of the TALDICE core, providing an extension back in time of the previous dating efforts (Bazin et al., 2013; Buiron et al., 2011; Schüpbach et al., 2011).

The age scale is built through the application of the IceChrono1 inverse model, which provides the best compromise between a background chronology and observations (tie points). We define gas matrix tie points for the oldest part of the core through the classic approach of manual wiggle matching between the new $\delta^{18}O_{atm}$ record of TALDICE and the $\delta^{18}O_{atm}$ profile of EDC. On the other hand, due to the absence of ice stratigraphic markers (e.g. volcanic tephra), we are forced to employ a non-conventional dating strategy, which includes the definition of ice age markers from TALDICE and EDC δD records for synchronization. In addition, we constrain the chronology through the application of the novel ^{81}Kr dating on three ice samples. Our study represents the first application of ^{81}Kr dating of about 5–10 kg of ice from a deep ice core to constrain the chronology. The dating effort for the deep portion of TALDICE demonstrates that the ice stratigraphy is preserved until 1548 m depth at an age of ~343 ka, i.e. in a zone where the thinning function reaches value close to 0, a value rarely observed in other deep ice cores. We cannot extend the chronology below 1548 m depth due to the lack of climatic variability in both δD and $\delta^{18}O_{atm}$ profiles. In addition, the ^{81}Kr dated samples indicate that below 1548 m the stratigraphy might be disturbed by mixing/folding process or by the presence of stagnant ice, as recently observed at Little Dome C (Lilien et al., 2021).

The TALDICE ice core can be now divided in three main sections: (i) between the top and 1438 m depth where the core age is defined by the AICC2012 chronology (Bazin et al., 2013), (ii) between 1438 m depth and 1548 m where the TALDICE-deep1 chronology applies and (iii) below 1548 m depth to the bottom (1620 m depth) a proper age scale cannot be defined due to lack of a clear preservation of the climatic signal.

Our new δD and $\delta^{18}O_{atm}$ records below 1438 m depth, provides the unique chance to investigate climate and environmental changes back to MIS 10.1 (~343 ka, 1548 m depth) in the Ross Sea sector of the EAIS. The comparison with other records from Plateau sites during interglacial periods identifies the existence of a different behaviour in the TALDICE δD record during MIS 7.5 and 9.3, as already observed for MIS 5.5 (Masson-Delmotte et al., 2011). Further research is needed to investigate this unique pattern.

Author contribution

Ilaria Crotti: conceptualization, investigation, writing – original draft. Amaelle Landais, Barbara Stenni: conceptualization, supervision, writing – review and editing. Lucie Bazin, Frédéric Parrenin: software, validation writing – review and editing. Massimo Frezzotti: writing – review and editing, supervision. Florian Ritterbusch, Zheng-Tian Lu, Wei Jiang, Guo-Min Yang: investigation, writing – review and editing. Elise Fourré, Anais Orsi, Roxanne Jacob, Bénédicte Minster, Frédéric Prié, Giuliano Dreossi: investigation. Carlo Barbante: supervision.

Data availability

The new data set produced in this study (δD 5 and 10 cm resolution data, $\delta^{18}O_{atm}$, $\delta^{15}N$ and $\delta O_2/N_2$) and the TALDICE-deep1 age scale is available at the Pangaea repository (https://www.pangaea.de/).

The IceChrono1 code is available in Python language at the following link https://github.com/parrenin/paleochrono. The EDC $\delta^{18}O_{atm}$ data are available at https://doi.pangaea.de/10.1594/PANGAEA.887327 . EDC δD data and the AICC2012 age scale can be found here https://doi.pangaea.de/10.1594/PANGAEA.824894.

Declaration of competing interest

The authors declare that they have no known competing financial interests or personal relationships that could have appeared to influence the work reported in this paper.

Acknowledgments

This work is part of the TALDEEP project funded by MIUR (PNRA18_00098). The Talos Dome Ice core Project (TALDICE), a joint European program, is funded by national contributions from Italy, France, Germany, Switzerland and the United Kingdom. Primary logistical support was provided by PNRA at Talos Dome. This is TALDICE publication no 60. The research leading to these results has also received funding from the European Research Council under the European Union H2020 Programme (H2020/20192024)/ ERC grant agreement no. 817493 ERC ICORDA.

This work is funded by the National Key Research and Development Program of China (2016YFA0302200), National Natural Science Foundation of China (41727901).

This publication was generated in the frame of Beyond EPICA. The project has received funding from the European Union's Horizon 2020 research and innovation programme under grant agreement No. 815384 (Oldest Ice Core). It is supported by national partners and funding agencies in Belgium, Denmark, France, Germany, Italy, Norway, Sweden, Switzerland, The Netherlands and the United Kingdom. Logistic support is mainly provided by ENEA and IPEV through the Concordia Station system. The opinions expressed and arguments employed herein do not necessarily reflect the official views of the European Union funding agency or other national funding bodies. This is Beyond EPICA publication number 20.

The author acknowledges funding from Università Italo-Francese / Université Franco-Italienne and the Vinci Scholarship for cotutorship Ph.D. program.

We also thank Antoine Grisart who contributed to this work analyzing the $\delta^{18}O_{atm}$ composition in 7 samples of the EDC core, which helped in refining TALDICE-deep1 chronology.

Appendix A. Gravitational and gas loss corrections

Gases and isotopes in the firn layer above the ice are mainly affected by gravitational separation above the ice (Craig et al., 1988). To correct $\delta^{18}O_{atm}$ measurements for the gravitational effect we use the $\delta^{15}N$ values obtained for the same samples applying the following formula:

$$\delta^{18}O_{atm\ corrected} = \delta^{18}O - 2\,\delta^{15}N \quad (A.1)$$

The factor of 2 arises from the fact that the gravitational effect is proportional to the mass difference between the two isotopes, meaning that it is two times larger for $\delta^{18}O$ ($^{18}O/^{16}O$) as for $\delta^{15}N$ ($^{15}N/^{14}N$) (Craig et al., 1988). $\delta O_2/N_2$ values are corrected as well for gravitational fractionation effects using $\delta^{15}N$ but with a factor of 4 as in the following equation (Extier et al., 2018):

$$\delta O_2 \,/\, N_{2\ corrected} = \delta O_2 \,/\, N_2 - 4\delta^{15}N \quad (A.2)$$

It has been demonstrated that the O_2/N_2 ratio of the ice sample decreases over time when ice is stored at temperatures higher than −50 °C, since O_2 is preferentially lost from clathrate hydrates through ice crystal after the coring in comparison to N_2 (Ikeda-Fukazawa et al., 2005; Kawamura et al., 2007; Landais et al., 2012).

The gas loss correction for $\delta^{18}O_{atm}$ is based on the measured $\delta O_2/N_2$ (Extier et al., 2018; Landais et al., 2003a, 2003b; Severinghaus et al., 2009) and follows the linear relationship:

$$\delta^{18}O_{atm\ corrected} = \delta^{18}O_{atm} + (\delta O_2 / N_2 + 10) \times 0.01 \quad (A.3)$$

This correction is estimated in two different ways. In Landais et al. (2003b), $\delta^{18}O_{atm}$ and $\delta O_2/N_2$ values are measured on neighboring Vostok ice core samples that are stored over different time periods. The second set of ice samples is stored 10 years longer at −20 °C than the first set of samples and an increase of $\delta^{18}O_{atm}$ by 0.3‰ is observed between the two series in parallel with a decrease of $\delta O_2/N_2$ of 30‰. In Severinghaus et al. (2009) and Extier et al. (2018), samples at the same depth are measured for $\delta^{18}O_{atm}$ and $\delta O_2/N_2$ with differences in $\delta O_2/N_2$ reaching 30‰. From paired difference plot for the $\delta^{18}O_{atm}$ vs $\delta O_2/N_2$, the same slope of 0.01 for variations of $\delta^{18}O_{atm}$ vs $\delta O_2/N_2$ due to gas loss are obtained. In the Extier et al. (2018) dataset, the $\delta O_2/N_2$ measurements from the EPICA Dome C ice core are performed in 2017 at the latest, i.e. after 13 years of storage at −20 °C. The $\delta O_2/N_2$ values measured for this series are on average −38 ± 18‰ with the most extreme value being a $\delta O_2/N_2$ of −78‰.

In our new dataset for the TALDICE samples, $\delta O_2/N_2$ are on average - 62 ± 25‰ with values down to −124‰ (Figure A.1). This is significantly less than what is observed for the EPICA Dome C or Vostok ice cores previously, and we can wonder if the same correction should be applied by extrapolating the results observed over variations of $\delta O_2/N_2$ over 30‰. Actually when we compare the new dataset obtained in 2020 and corrected with equation (A.3), with data obtained in 2011 and 2012, corrected with the same equation and published in Bazin et al. (2013), we observe a huge scatter. We hypothesize that the gas loss correction extrapolated from Extier et al. (2018) to values of $\delta O_2/N_2$ lower than −100‰ is too strong. We calculate a mean decrease of about 7.30‰ between 2011 and 2012 series and of 48.88‰ between 2011 and 2019 series. In order to revise this correction for low $\delta O_2/N_2$ values, we thus explore again the EPICA Dome C raw data obtained in Extier et al. (2018) extracting the neighboring samples and showing differences of $\delta O_2/N_2$ larger than 40‰ (Table A.1). It is not possible to have neighboring samples with exactly the same depth with such a high $\delta O_2/N_2$ difference, but we find high $\delta O_2/N_2$ difference for EDC samples with a depth difference of less than 2 m. Comparison of $\delta^{18}O_{atm}$ and $\delta O_2/N_2$ values between samples taken at less than 2 m depth difference is justified by the fact that natural $\delta^{18}O_{atm}$ and $\delta O_2/$

N_2 variations occur on long-time (orbital) scale while our samples are chosen on a depth range where 1 m records less than 500 years of climatic history.

The slope for these EDC samples that experienced extreme gas loss is only 0.007, thus only 70% of the classical slope for more moderate gas loss (0.01) Equation (A.3). For TALDICE samples associated with a $\delta O_2/N_2$ lower than −50‰, we thus apply the following equation instead of the classical one:

$$\delta^{18}O_{atm\ corrected} = \delta^{18}O_{atm} + (\delta O_2 / N_2 + 10) \times 0.007 \quad (A.4)$$

Table A.1
EPICA Dome C raw data obtained in Extier et al. (2018) extracting the neighboring samples showing differences of $\delta O_2/N_2$ larger than 40‰. Data comparison allows the calculation of the average slope equal to 0.007 to correct $\delta^{18}O_{atm}$ data with $\delta O_2/N_2$ values lower than - 50‰.

Depth (m)	$\delta O_2/N_2$ (‰)	$\delta^{18}O_{atm}$(‰)	Ratio $\Delta\delta^{18}O_{atm}$ vs $\Delta\delta O_2/N_2$
2315.473	−8	1.70	−0.009
2316.628	−52	2.11	
2352.873	−7	1.41	−0.006
2353.450	−66	1.79	
2357.850	−57	1.60	−0.007
2358.923	−8	1.26	
2346.823	−9	1.51	−0.006
2346.850	−56	1.77	
2433.750	−45	1.24	−0.008
2435.373	−5	0.91	
2334.750	−52	1.88	−0.006
2335.273	−12	1.65	
2363.350	−58	1.52	−0.005
2364.423	−7	1.25	

Average slope $\Delta\delta^{18}O_{atm}$ vs $\Delta\delta O_2/N_2 = -0.007$.

Appendix B. ^{81}Kr and uncertainty calculation

The ^{81}Kr abundance R_{81} in the sample is determined by the number of counted ^{81}Kr atoms in the sample as compared to the atmospheric reference. If ^{85}Kr is found to be present in the sample, indicating contamination of modern krypton, then correction must be applied to the measured ^{81}Kr abundance. The measured ^{85}Kr activity in the TALDICE samples is below the detection limit, so no correction is applied. If the ^{81}Kr abundance in the atmosphere had been constant in the past, the ^{81}Kr-age would simply be:

$$^{81}Kr - age = -t_{1/2} \Big/ \ln(2) \ln(R_{81}) \quad (B.1)$$

where $t_{1/2}$= (229 ± 11 ka) is the half-life of ^{81}Kr. However, the ^{81}Kr abundance in the atmosphere has not been completely constant in the past due to variations of the cosmic ray flux on the earth which lead to a potential difference in the ^{81}Kr-age of up to 4% (Buizert et al., 2014; Zappala et al., 2020). As the atmospheric ^{81}Kr abundance of the past 1.5 Ma can be calculated based on reconstructions of the relative geomagnetic field intensity, the atmospheric ^{81}Kr input history can be taken into account when calculating the ^{81}Kr-age. This is done for the ^{81}Kr-ages of the TALDICE samples given in Table 1.

The error of the measured ^{81}Kr abundance is given by the statistical error of the atom counting. This error propagates to the ^{81}Kr-age, also taking into account the ^{81}Kr input history. Due to this reason, and because the relation between the ^{81}Kr-age and the ^{81}Kr abundance is not linear, the error of the ^{81}Kr-age can be asymmetric. Due to the uncertainty of the ^{81}Kr half-life, there is an additional systematic error on the ^{81}Kr-age. This systematic error would affect all the ^{81}Kr-ages in the same way, so that they would shift up or down together.

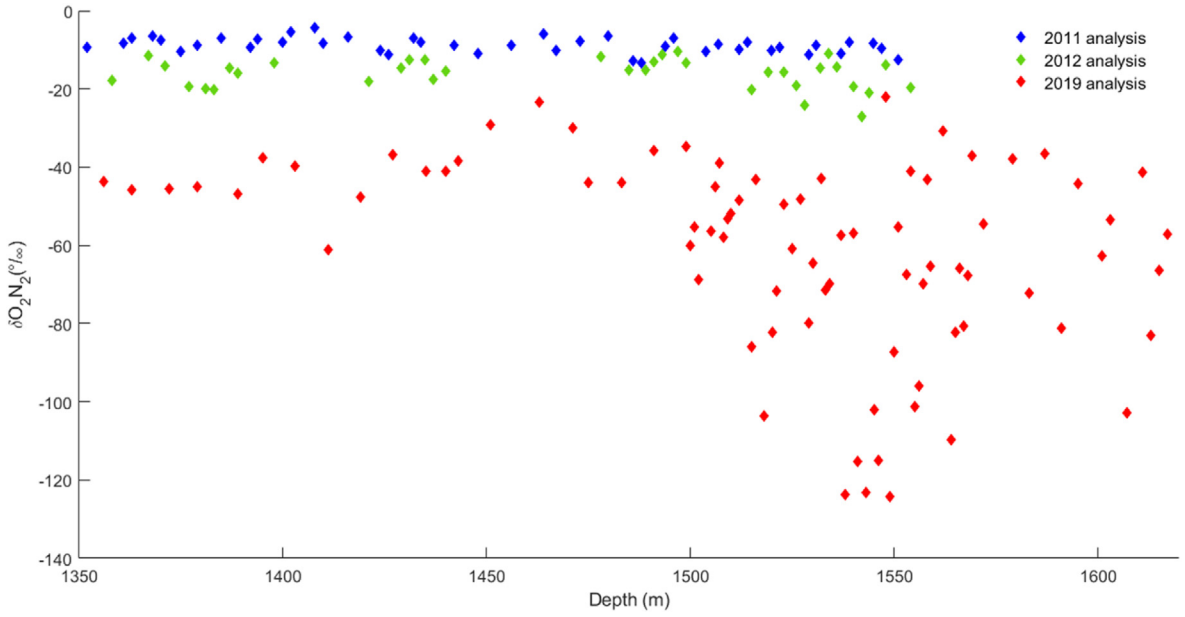

Fig. A.1. $\delta O_2/N_2$ measurements for the TALDICE core between 1350 m and 1620 m depth performed in 2011 (blue diamonds), 2012 (green diamonds) and 2019 (red diamonds).

Appendix C. Uncertainties calculation on IceChrono1 model input files

In this section we describe how we calculate the uncertainties associated with the background scenario quantities and with the air-ice stratigraphic links. Our background scenario is made by the thinning function and the accumulation rate quantities defined by Buiron et al. (2011) with 1D ice flow model, while the LID is derived from the new $\delta^{15}N$ data set.

Considering the difficulties encountered in the definition of the background scenario for the deep portion of TALDICE core, due to the poorly constrained 1D ice flow model, we choose to define relative uncertainties as constant values and larger with respect to the values of thinning function and accumulation rate, hence respectively equal to $\sigma = 1$ and $\sigma = 0.5$. This strategy, already applied by Bazin et al. (2013), allows the IceChrono1 model to base the output chronology on the stratigraphic links and on the LIDIE, rather than on the glaciological quantities. On the other hand, the LIDIE relative uncertainty is carefully calculated at each depth level. At first we calculate the uncertainty as the absolute difference between the LIDIE obtained for the TALDICE-1 background chronology (Buiron et al., 2011) and then we transform it in relative uncertainty (*ru*), which is calculated through the following formula:

$$ru = \ln[(x+\sigma) / (x-\sigma)] / 2 \quad \text{(C.1)}$$

where x is value of LIDIE associated with a certain depth and σ is its uncertainty.

We compute the uncertainties for the gas and ice stratigraphic links (tie points) as well. We calculate for each tie point the cumulative uncertainty (*cu*), which follows the equation above:

$$cu = \left(\sigma_{ID}{}^2 + res^2 + \sigma_{ref}{}^2\right)^{1/2} \quad \text{(C.2)}$$

where σ_{ID} is the difference between the maximum and the minimum age associated with the single tie point, *res* is the *a priori* temporal resolution of the record estimated from theTADICE-1 age scale and σ_{ref} is the uncertainty associated with AICC2012 gas or ice age scale for the EDC core.

References

Aoki, N., Makide, Y., 2005. The concentration of krypton in the atmosphere — its revision after half a century —. https://doi.org/10.1246/cl.2005.1396, 34, 10, 10-11.

Bazin, L., Landais, A., Lemieux-Dudon, B., Toyé Mahamadou Kele, H., Veres, D., Parrenin, F., Martinerie, P., Ritz, C., Capron, E., Lipenkov, V., Loutre, M.F., Raynaud, D., Vinther, B., Svensson, A., Rasmussen, S.O., Severi, M., Blunier, T., Leuenberger, M., Fischer, H., Wolff, E., 2013. An optimized multi-proxy, multi-site Antarctic ice and gas orbital chronology (AICC2012): 120-800 ka. Clim. Past 9 (4), 1715–1731. https://doi.org/10.5194/cp-9-1715-2013.

Bradley, S.L., Siddall, M., Milne, G.A., Masson-Delmotte, V., Wolff, E., 2012. Where might we find evidence of a Last Interglacial West Antarctic Ice Sheet collapse in Antarctic ice core records? Global Planet. Change 88 (89), 64–75. https://doi.org/10.1016/j.gloplacha.2012.03.004.

Bréant, C., Martinerie, P., Orsi, A., Arnaud, L., Landais, A., 2017. Modelling firn thickness evolution during the last deglaciation: constraints on sensitivity to temperature and impurities. Clim. Past 13, 833–853. https://doi.org/10.5194/cp-13-833-2017.

Buiron, D., Chappellaz, J., Stenni, B., Frezzotti, M., Baumgartner, M., Capron, E., Landais, A., Lemieux-Dudon, B., Masson-Delmotte, V., Montagnat, M., Parrenin, F., Schilt, A., 2011. TALDICE-1 age scale of the Talos Dome deep ice core, East Antarctica. Clim. Past 7 (1), 1–16. https://doi.org/10.5194/cp-7-1-2011.

Buizert, C., Baggenstos, D., Jiang, W., Purtschert, R., Petrenko, V.V., Lu, Z.T., Müller, P., Kuhl, T., Lee, J., Severinghaus, J.P., Brook, E.J., 2014. Radiometric 81Kr dating identifies 120,000-year-old ice at Taylor Glacier, Antarctica. Proc. Natl. Acad. Sci. U.S.A. 111 (19), 6876–6881. https://doi.org/10.1073/pnas.1320329111.

Buizert, C., Sowers, T., Blunier, T., 2013. Assessment of diffusive isotopic fractionation in polar firn, and application to ice core trace gas records. Earth Planet Sci. Lett. 361, 110–119. https://doi.org/10.1016/j.epsl.2012.11.039.

Capron, E., Landais, A., Lemieux-Dudon, B., Schilt, A., Masson-Delmotte, V., Buiron, D., Chappellaz, J., Dahl-Jensen, D., Johnsen, S., Leuenberger, M., Loulergue, L., Oerter, H., 2010. Synchronising EDML and NorthGRIP ice cores using δ18O of atmospheric oxygen (δ18Oatm) and CH4 measurements over MIS5 (80-123 kyr). Quat. Sci. Rev. 29 (1–2), 222–234. https://doi.org/10.1016/j.quascirev.2009.07.014.

Craig, H., Horibe, Y., Sowers, T., 1988. Gravitational separation of gases and isotopes in polar ice caps. Science 242 (4886), 1675–1678. https://doi.org/10.1126/science.242.4886.1675.

Dong, X.Z., Ritterbusch, F., Chu, Y.Q., Gu, J.Q., Hu, S.M., Jiang, W., Lu, Z.T., Yang, G.M., Zhao, L., 2019. Dual separation of krypton and argon from environmental samples for radioisotope dating. Anal. Chem. 91 (21), 13576–13581. https://doi.org/10.1021/acs.analchem.9b02716.

Dreyfus, G.B., Parrenin, F., Lemieux-Dudon, B., Durand, G., Masson-Delmotte, V., Jouzel, J., Barnola, J.M., Panno, L., Spahni, R., Tisserand, A., Siegenthaler, U., Leuenberger, M., 2007. Anomalous flow below 2700 m in the EPICA Dome C ice core detected using δ18O of atmospheric oxygen measurements. Clim. Past 3 (2), 341–353. https://doi.org/10.5194/cp-3-341-2007.

EPICA community members, 2004. Eight glacial cycles from an Antarctic ice core. Nature 429 (1), 623–628. https://doi.org/10.1016/S0921-8181(99)00023-5.

Extier, T., Landais, A., Bréant, C., Prié, F., Bazin, L., Dreyfus, G., Roche, D.M., Leuenberger, M., 2018. On the use of δ18Oatm for ice core dating. Quat. Sci. Rev. 185, 244–257. https://doi.org/10.1016/j.quascirev.2018.02.008.

Frezzotti, M., Bitelli, G., De Michelis, P., Deponti, A., Forieri, A., Gandolfi, S., Maggi, V., Mancini, F., Remy, F., Tabacco, I.E., Urbini, S., Vittuari, L., Zirizzottl, A., 2004. Geophysical survey at Talos Dome, East Antarctica: the search for a new deep-drilling site. Ann. Glaciol. 39 (2002), 423–432. https://doi.org/10.3189/172756404781814591.

Goujon, C., Barnola, J.M., Ritz, C., 2003. Modelling the densification of polar firn including heat diffusion: application to close-off characteristics and gas isotopic fractionation for Antarctica and Greenland sites. J. Geophys. Res. 108 (24), 1–18. https://doi.org/10.1029/2002jd003319. In this issue.

Herron, M., Langway, C., 1980. Firn densification: an empirical model. J. Glaciol. 25 (93), 373–385.

Ikeda-Fukazawa, T., Fukumizu, K., Kawamura, K., Aoki, S., Nakazawa, T., Hondoh, T., 2005. Effects of molecular diffusion on trapped gas composition in polar ice cores. Earth Planet Sci. Lett. 229 (3–4), 183–192. https://doi.org/10.1016/j.epsl.2004.11.011.

Jiang, W., Bailey, K., Lu, Z.T., Mueller, P., O'Connor, T.P., Cheng, C.F., Hu, S.M., Purtschert, R., Sturchio, N.C., Sun, Y.R., Williams, W.D., Yang, G.M., 2012. An atom counter for measuring 81Kr and 85Kr in environmental samples. Geochem. Cosmochim. Acta 91, 1–6. https://doi.org/10.1016/j.gca.2012.05.019.

Jiang, Wei, Hu, S.M., Lu, Z.T., Ritterbusch, F., Yang, G. min, 2020. Latest development of radiokrypton dating – a tool to find and study paleogroundwater. Quat. Int. 547 (April 2019), 166–171. https://doi.org/10.1016/j.quaint.2019.04.025.

Jordan, T., Ferraccioli, F., Corr, H., Robinson, C., Caneva, G., Armadillo, E., Bozzo, E., Frearson, N., 2008. Linking the Wilkes Subglacial Basin the transantarctic Mountains and the Ross Sea with a new airborne gravity survey. Terra Antarctica Reports 13, 37–54.

Kawamura, K., Parrenin, F., Lisiecki, L., Uemura, R., Vimeux, F., Severinghaus, J.P., Hutterli, M.A., Nakazawa, T., Aoki, S., Jouzel, J., Raymo, M.E., Matsumoto, K., Nakata, H., Motoyama, H., Fujita, S., Goto-Azuma, K., Fujii, Y., Watanabe, O., 2007. Northern Hemisphere forcing of climatic cycles in Antarctica over the past 360,000 years. Nature 448 (7156), 912–916. https://doi.org/10.1038/nature06015.

Landais, A., Barnola, J.M., Kawamura, K., Caillon, N., Delmotte, M., Van Ommen, T., Dreyfus, G., Jouzel, J., Masson Delmotte, V., Minster, B., Freitag, J., Leuenberger, M., Schwander, J., Huber, C., Etheridge, D., Morgan, V., 2006. Firn-air δ15N in modern polar sites and glacial-interglacial ice: a model-data mismatch during glacial periods in Antarctica? Quat. Sci. Rev. 25 (1–2), 49–62. https://doi.org/10.1016/j.quascirev.2005.06.007.

Landais, A., Caillon, N., Severinghaus, J.P., Jouzel, J., Masson-Delmotte, V., 2003a. Analyses isotopiques à haute précision de l'air piégé dans les glaces polaires pour la quantification des variations de température: methode et limites. Notes Des Activités Instrumentales de l'IPSL 39.

Landais, A., Chappellaz, J., Delmotte, M., Jouzel, J., Blunier, T., Bourg, C., Caillon, N., Cherrier, S., Malaizé, B., Masson-Delmotte, V., Raynaud, D., Schwander, J., Steffensen, J.P., 2003b. A tentative reconstruction of the last interglacial and glacial inception in Greenland based on new gas measurements in the Greenland Ice Core Project (GRIP) ice core. J. Geophys. Res.: Atmosphere 108 (18). https://doi.org/10.1029/2002jd003147.

Landais, A., Dreyfus, G., Capron, E., Pol, K., Loutre, M.F., Raynaud, D., Lipenkov, V.Y., Arnaud, L., Masson-Delmotte, V., Paillard, D., Jouzel, J., Leuenberger, M., 2012. Towards orbital dating of the EPICA Dome C ice core using δO 2/N 2. Clim. Past 8 (1), 191–203. https://doi.org/10.5194/cp-8-191-2012.

Lemieux-Dudon, B., Blayo, E., Petit, J.R., Waelbroeck, C., Svensson, A., Ritz, C., Barnola, J.M., Narcisi, B.M., Parrenin, F., 2010. Consistent dating for Antarctic and Greenland ice cores. Quat. Sci. Rev. 29 (1–2), 8–20. https://doi.org/10.1016/j.quascirev.2009.11.010.

Lilien, D.A., Steinhage, D., Taylor, D., Parrenin, F., Ritz, C., Mulvaney, R., Martín, C., Yan, J.B., O'Neill, C., Frezzotti, M., Miller, H., Gogineni, P., Dahl Jensen, D., Eisen, O., 2021. Brief communication: new radar constraints support presence of ice older than 1.5 Myr at Little Dome C. Cryosphere 15 (4), 1881–1888. https://doi.org/10.5194/tc-15-1881-2021.

Lisiecki, L.E., Raymo, M.E., 2005. A Pliocene-Pleistocene stack of 57 globally

distributed benthic δ 18O records. Paleoceanography 20 (1), 1–17. https://doi.org/10.1029/2004PA001071.
Loosli, H.H., Oeschger, H., 1969. 37Ar and 81Kr in the atmosphere. Earth Planet Sci. Lett. 7, 67–71.
Loulergue, L., Schilt, A., Spahni, R., Masson-Delmotte, V., Blunier, T., Lemieux, B., Barnola, J.M., Raynaud, D., Stocker, T.F., Chappellaz, J., 2008. Orbital and millennial-scale features of atmospheric CH4 over the past 800,000 years. Nature 453 (7193), 383–386. https://doi.org/10.1038/nature06950.
Lu, Z.T., Schlosser, P., Smethie, W.M., Sturchio, N.C., Fischer, T.P., Kennedy, B.M., Purtschert, R., Severinghaus, J.P., Solomon, D.K., Tanhua, T., Yokochi, R., 2014. Tracer applications of noble gas radionuclides in the geosciences. Earth Sci. Rev. 138, 196–214. https://doi.org/10.1016/j.earscirev.2013.09.002.
Magand, O., Frezzotti, M., Pourchet, M., Stenni, B., Genoni, L., Fily, M., 2004. Climate variability along latitudinal and longitudinal transects in East Antarctica. Ann. Glaciol. 39, 351–358. https://doi.org/10.3189/172756404781813961.
Masson-Delmotte, V., Buiron, D., Ekaykin, A., Frezzotti, M., Gallée, H., Jouzel, J., Krinner, G., Landais, A., Motoyama, H., Oerter, H., Pol, K., Pollard, D., Ritz, C., Schlosser, E., Sime, L.C., Sodemann, H., Stenni, B., Uemura, R., Vimeux, F., 2011. A comparison of the present and last interglacial periods in six Antarctic ice cores. Clim. Past 7 (2), 397–423. https://doi.org/10.5194/cp-7-397-2011.
Montagnat, M., Buiron, D., Arnaud L, L., Broquet, A., Schlitz, P., Jacob, R., Kipfstuhl, S., 2012. Measurements and numerical simulation of fabric evolution along the Talos Dome ice core , Antarctica. Earth Planet Sci. Lett. 357-358, 168–178. https://doi.org/10.1016/j.epsl.2012.09.025.
Morlighem, M., Rignot, E., Binder, T., Blankenship, D., Drews, R., Eagles, G., Eisen, O., Ferraccioli, F., Forsberg, R., Fretwell, P., Goel, V., Greenbaum, J., Gudmundsson, H., Guo, J., Helm, V., Hofstede, C., Howat, I., Humbert, A., Jokat, W., Karlsson, N., Lee, W.S., Matsuoka, K., Millan, R., Mouginot, J., Paden, J., Pattyn, F., Roberts, J., Rosier, S., Ruppel, A., Seroussi, H., Smith, E., Steinhage, D., Sun, B., Van den Broeke, M., Van Ommen, T., Van Wessem, M., Young, D., 2020. Deep glacial troughs and stabilizing ridges unveiled beneath the margins of the Antarctic ice sheet. Nat. Geosci. 13 (2), 132–137. https://doi.org/10.1038/s41561-019-0510-8.
NEEM community members, 2013. Eemian interglacial reconstructed from a Greenland folded ice core. Nature 493, 489–494. https://doi.org/10.1038/nature11789.
Parrenin, F., Barker, S., Blunier, T., Chappellaz, J., Jouzel, J., Landais, A., Masson-Delmotte, V., Schwander, J., Veres, D., 2012. On the gas-ice depth difference (Δdepth) along the EPICA Dome C ice core. Clim. Past 8 (4), 1239–1255. https://doi.org/10.5194/cp-8-1239-2012.
Parrenin, F., Bazin, L., Capron, E., Landais, A., Lemieux-Dudon, B., Masson-Delmotte, V., 2015. IceChrono1: a probabilistic model to compute a common and optimal chronology for several ice cores. Geosci. Model Dev. (GMD) 8 (5), 1473–1492. https://doi.org/10.5194/gmd-8-1473-2015.
Parrenin, F., Cavitte, M.G.P., Blankenship, D.D., Chappellaz, J., Fischer, H., Gagliardini, O., Masson-Delmotte, V., Passalacqua, O., Ritz, C., Roberts, J., Siegert, M.J., Young, D.A., 2017. Is there 1.5-million-year-old ice near Dome C, Antarctica? Cryosphere 11 (6), 2427–2437. https://doi.org/10.5194/tc-11-2427-2017.
Parrenin, F., Dreyfus, G., Durand, G., Fujita, S., Gagliardini, O., Gillet, F., Jouze, J., Kawamura, K., Lhomme, N., Masson-Delmotte, V., Ritz, C., Schwander, J., Shoji, H., Uemura, R., Watanabe, O., Yoshida, N., 2007. 1-D-ice flow modelling at EPICA dome C and dome Fuji, East Antarctica. Clim. Past 3 (2), 243–259. https://doi.org/10.5194/cp-3-243-2007.
Parrenin, F., Rémy, F., Ritz, C., Siegert, M.J., Jouzel, J., 2004. New modeling of the Vostok ice flow line and implication for the glaciological chronology of the Vostok ice core. J. Geophys. Res. Atmos. 109 (20) https://doi.org/10.1029/2004JD004561.
Petit, J.R., Jouzel, J., Raynaud, D., Barkov, N.I., Barnola, J.M., Basile, I., Bender, M., Chappellaz, J., Davis, M., Delaygue, G., Delmotte, M., Kotiyakov, V.M., Legrand, M., Lipenkov, V.Y., Lorius, C., Pépin, L., Ritz, C., Saltzman, E., Stievenard, M., 1999. Climate and atmospheric history of the past 420,000 years from the Vostok ice core, Antarctica. Nature 399 (6735), 429–436. https://doi.org/10.1038/20859.
Raynaud, D., Jouzel, J., Delmas, R., 1993. The ice record of greenhouse gases. Science 259 (5097), 926–934. https://doi.org/10.1126/science.259.5097.926.
Schüpbach, S., Federer, U., Bigler, M., Fischer, H., Stocker, T.F., 2011. A refined TALDICE-1a age scale from 55 to 112 ka before present for the Talos Dome ice core based on high-resolution methane measurements. Clim. Past 7 (3), 1001–1009. https://doi.org/10.5194/cp-7-1001-2011.
Severinghaus, J.P., Beaudette, R., Headly, M.A., Taylor, K., Brook, E.J., 2009. Oxygen-18 of O2 records the impact of abrupt climate change on the terrestrial biosphere. Science 324 (5933), 1431–1434. https://doi.org/10.1126/science.1169473.
Severinghaus, J.P., Sowers, T., Brook, E.J., Alley, R.B., Bender, M.L., 1998. Timing of abrupt climate change at the end of the younger dryas interval from thermally fractionated gases in polar ice. Nature 391 (6663), 141–146. https://doi.org/10.1038/34346.
Sowers, T., Bender, M., Raynaud, D., Korotkevich, Y.S., 1992. δ15N of N2 in air trapped in polar ice: a tracer of gas transport in the firn and a possible constraint on ice age-gas age differences. J. Geophys. Res. 97 (D14) https://doi.org/10.1029/92jd01297.
Stenni, B., Buiron, D., Frezzotti, M., Albani, S., Barbante, C., Bard, E., Barnola, J.M., Baroni, M., Baumgartner, M., Bonazza, M., Capron, E., Castellano, E., Chappellaz, J., Delmonte, B., Falourd, S., Genoni, L., Iacumin, P., Jouzel, J., Kipfstuhl, S., Udisti, R., 2011. Expression of the bipolar see-saw in Antarctic climate records during the last deglaciation. Nat. Geosci. 4 (1), 46–49. https://doi.org/10.1038/ngeo1026.
Tian, L., Ritterbusch, F., Gu, J.Q., Hu, S.M., Jiang, W., Lu, Z.T., Wang, D., Yang, G.M., 2019. 81Kr dating at the Guliya ice Cap, Tibetan plateau. Geophys. Res. Lett. 46 (12), 6636–6643. https://doi.org/10.1029/2019GL082464.
Tison, J.-L., Barnola, J.-M., Petit, J.-R., 2015. Retrieving the paleoclimatic signal from the deeper part of the EPICA Dome C ice core. Cryosphere 9 (4), 1633–1648. https://doi.org/10.5194/tc-9-1633-2015-supplement.
Uemura, R., Motoyama, H., Masson-Delmotte, V., Jouzel, J., Kawamura, K., Goto-Azuma, K., Fujita, S., Kuramoto, T., Hirabayashi, M., Miyake, T., Ohno, H., Fujita, K., Abe-Ouchi, A., Iizuka, Y., Horikawa, S., Igarashi, M., Suzuki, K., Suzuki, T., Fujii, Y., 2018. Asynchrony between Antarctic temperature and CO 2 associated with obliquity over the past 720,000 years. Nat. Commun. 9 (1), 1–11. https://doi.org/10.1038/s41467-018-03328-3.
Urbini, S., Frezzotti, M., Gandolfi, S., Vincent, C., Scarchilli, C., Vittuari, L., Fily, M., 2008. Historical behaviour of Dome C and Talos Dome (East Antarctica) as investigated by snow accumulation and ice velocity measurements. Global Planet. Change 60 (3–4), 576–588. https://doi.org/10.1016/j.gloplacha.2007.08.002.
Veres, D., Bazin, L., Landais, A., Toyé Mahamadou Kele, H., Lemieux-Dudon, B., Parrenin, F., Martinerie, P., Blayo, E., Blunier, T., Capron, E., Chappellaz, J., Rasmussen, S.O., Severi, M., Svensson, A., Vinther, B., Wolff, E.W., 2013. The Antarctic ice core chronology (AICC2012): an optimized multi-parameter and multi-site dating approach for the last 120 thousand years. Clim. Past 9 (4), 1733–1748. https://doi.org/10.5194/cp-9-1733-2013.
Zappala, J.C., Baggenstos, D., Gerber, C., Jiang, W., Kennedy, B.M., Lu, Z.T., Masarik, J., Mueller, P., Purtschert, R., Visser, A., 2020. Atmospheric 81Kr as an integrator of cosmic-ray flux on the hundred-thousand-year time scale. Geophys. Res. Lett. 47 (3), 1–7. https://doi.org/10.1029/2019GL086381.